Comparison of Developing vs Non-Developing Tropical Disturbances

by
Steven L. Erickson

Department of Atmospheric Science
Colorado State University
Fort Collins, Colorado

Colorado State University

Department of Atmospheric Science

Paper No. 274

COMPARISON OF DEVELOPING VS. NON-DEVELOPING TROPICAL DISTURBANCES

by

Steven L. Erickson

Department of Atmospheric Science

Colorado State University

Fort Collins, Colorado

July, 1977

Atmospheric Science Paper No. 274

TABLE OF CONTENTS

ABSTRACT

Developing and non-developing western North Pacific tropical disturbances are investigated and compared utilizing Defense Meteorological Satellite Program (DMSP) and rawinsonde data. Quantitative measurements of deep convection and cirrus amounts from the satellite visual and infrared data indicates that no large deep-convective difference exists between these two classes of disturbances. In addition, the daily variability of deep convection was determined to be large in both the developing and non-developing disturbances. Implications are that the amount and intensity of deep convection is not well related to disturbance tropical storm genesis potential. Genesis appears to be related to the special positioning of the deep convection and surrounding wind fields. When genesis occurs, the deep convection appears to act indirectly to warm the tropical disturbance by means of dynamically forced subsidence. Documentation is provided to support this hypothesis.

Relative vorticity, vertical shear and characteristics of the cirrus level outflow patterns were determined to be parameters which displayed the largest difference between the two classes of developing and non-developing disturbances. It is hypothesized that the potential for tropical disturbance genesis is primarily related to: 1) the large-scale surrounding relative vorticity at lower and upper tropospheric levels, 2) the strength of the disturbance's dynamically forced subsidence, and 3) the magnitude of disturbance ventilation or wind blow-through.

1. INTRODUCTION

1.1 Background

The climatological and statistical requirements for cyclone genesis have been summarized and discussed by Gray (1968, 1975). Much less understood, but of fundamental importance to genesis, are the daily physical differences between tropical disturbances which intensify and those which do not. It is apparent that tropical cyclones evolve out of a pre-existing tropical disturbance (Riehl, 1954) or cloud clusters[1], a meteorological term adopted from the visual appearance of cloud systems on the early satellite data of the mid to late 1960's. The most striking feature of the cloud cluster is the reflected solar radiation measured from deep penetrative convection and the associated cirrus canopies.

The early meteorological satellites were recognized as a valuable observational platform in the analysis of tropical disturbances (Sadler, 1967). Studies by Fett (1966), Fritz et al. (1966), Hubert and Timchalk (1969), and Dvorak (1973, 1975) have advanced techniques on estimating cyclone intensity based upon visual cloud features. Fett and Brand (1975) have proposed a method of forecasting cyclone movement based upon satellite observations. Improved sensors aboard recent satellites have also made it possible to obtain quantitative cloud information. Sikdar et al. (1970) determined the convective transport of mass based

[1]The term cloud cluster will not be used synonymously with tropical weather systems in this study. Whenever the term cloud cluster is used, the definition adopted by the GARP committee in 1968 will be adhered to. The high resolution satellite data used in this study indicates tropical weather disturbances are usually made up of several groups of clouds in cluster form.

on a brightness technique. A similar approach has been utilized to determine the cirrus outflow divergence of tropical cloud clusters (Fraedrich et al., 1976). The satellite has proven to be an invaluable observing platform in the day to day operational environment. Advanced technology has also made it an indispensable source of data for the research scientist. However, an important question remains unanswered. Can the meteorological satellite be used to distinguish between developing and non-developing tropical disturbances?

1.2 Purpose

The purpose of this study is to compare western North Pacific tropical disturbances which develop into tropical cyclones with those which do not. Comparisons are made to determine the physical processes which differentiate these systems. The Defense Meteorological Satellite Program (DMSP) visual and infrared film transparencies are processed utilizing the Colorado State University Optical Data Digitizer and Display System (OD^3) to yield quantitative area measurements of penetrative cumulus convection and their associated cirrus canopies. A description of the average disturbance and its day to day variability is made. Upper-level (cirrus) wind patterns are determined from diverging cirrus streaks on the visual satellite data.

A rawinsonde compositing technique (Williams and Gray, 1973; Ruprecht and Gray, 1976; George and Gray, 1976; Frank, 1976; and Zehr, 1976) was also applied to the disturbances and provided an independent data set to compare with the satellite observations. Rawinsonde composite results also specified key genesis parameters which could not be determined in the satellite analysis. Important differences and

similarities between developing and non-developing disturbances as specified by the satellite and rawinsonde analyses are discussed. In particular, the probable role played by deep convection in initiating the warm core vortex is discussed.

2. TECHNIQUE

Satellite film transparencies used in this study were obtained from Guam and the University of Wisconsin Space Science and Engineering Center, DMSP satellite archive section. This was a classified satellite until 1971. The transparencies were originally processed by the direct readout DMSP site located at Nimitz Hill, Guam in support of the Joint Typhoon Warning Center (JTWC). The high resolution DMSP data is unique and of superior resolution as compared to current civilian satellite pictures. Area measurements of deep convection were made using the visual Very High Resolution (VHR) transparencies (.33 n mi = .62 km resolution at subpoint). Mode Infrared (MI) transparencies (2 n mi = 3.7 km resolution at subpoint), taken simultaneously with the visual signal, were used to obtain area measurements of the cirrus canopies. Figure 1 shows a typical example of the visual (gridded) and infrared transparency data. Satellite gridding procedures are explained in Appendix A. For additional information on DMSP satellites and data, the reader is referred to Dickinson et al. (1974).

2.1 Criteria for selecting developing and non-developing disturbances

This study was limited to the investigation of only those developing and non-developing disturbances which originated in or near the western North Pacific Inter-Tropical Convergence Zone (ITCZ). Trade wind or so called embedded genesis characteristic of higher latitude cyclone formation is not treated. The developing and non-developing disturbances are referred to as ES1 (Early Stage 1) and 00', respectively. Figure 2 shows the initial position of the developing (O's) and non-developing (X's) disturbance cases. Table 1 gives the total

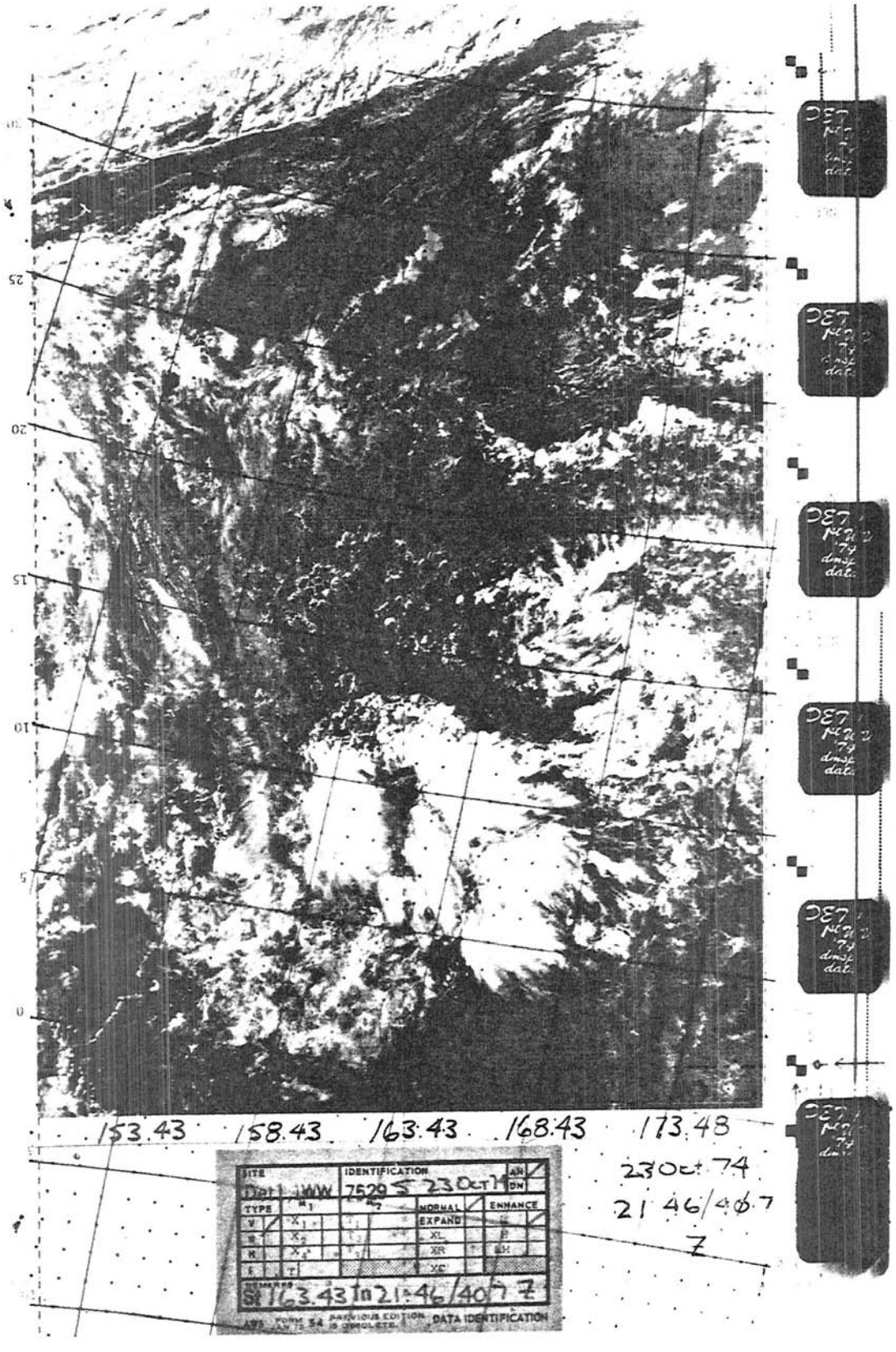

Fig. 1a. An example of a DMSP visual (gridded) transparency with a typical tropical disturbance located near 10°N, 163°E. See Appendix A for gridding procedures.

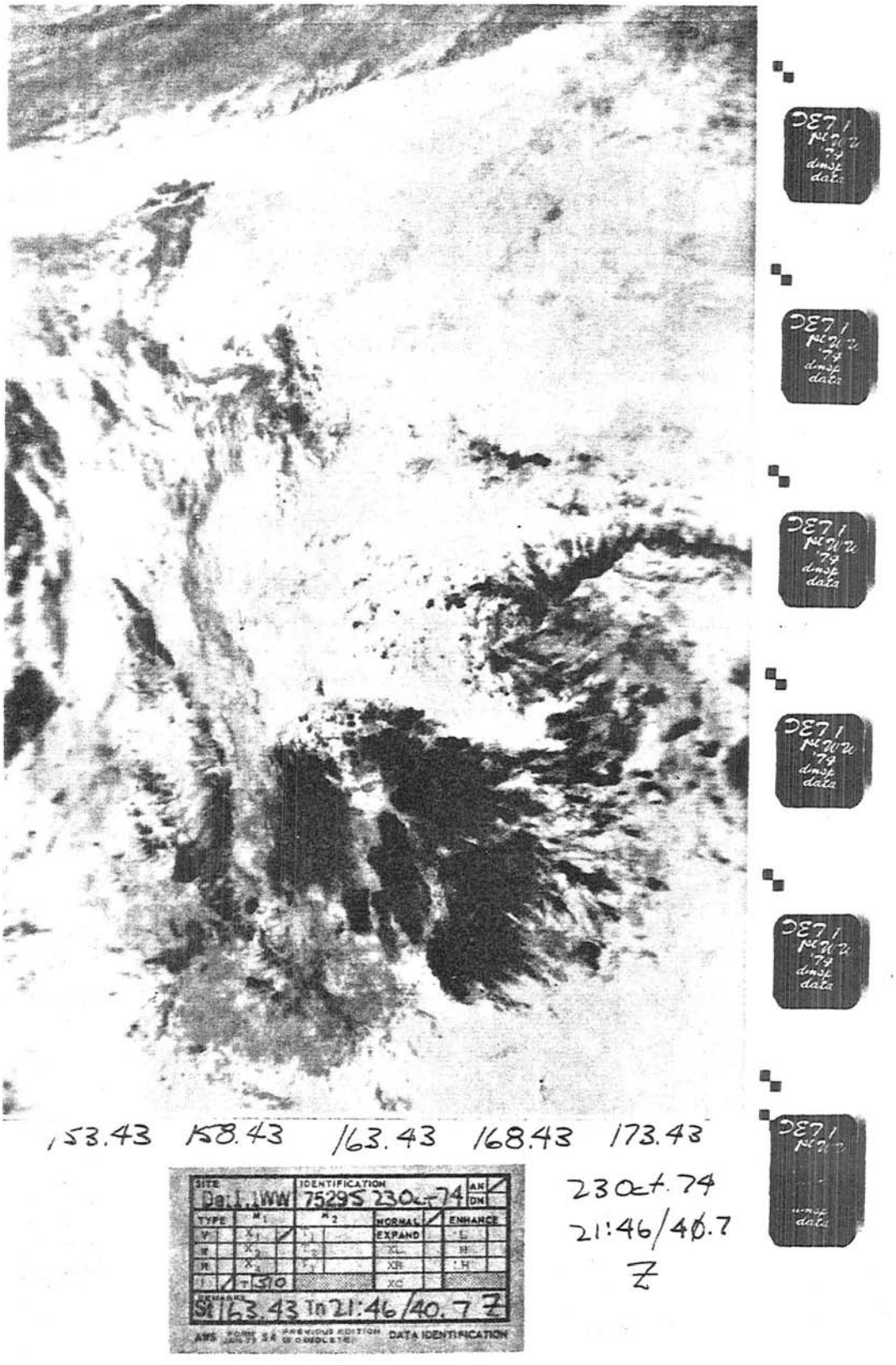

Fig. 1b. An example of a DMSP infrared film transparency which corresponds directly to Fig. 1a. Longitude and time of nodal crossing are listed in legend (i.e., 163,4°E and 21:46 GMT).

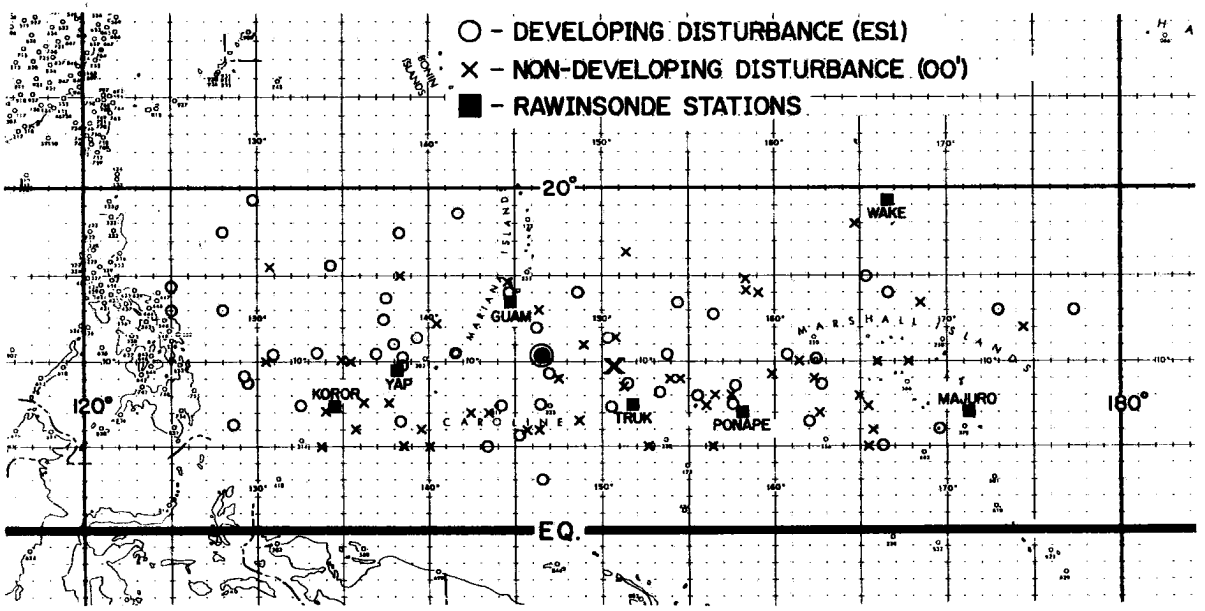

Fig. 2. X's and O's mark the initial position of the non-developing (OO') and developing (ES1) disturbances, respectively. The centroids of these positions are denoted by the large X (non-developing) and the large O (developing).

TABLE 1

Sample Sizes of the Developing and Non-developing Disturbances

	Non-developing (00')	Developing (ES1)
Total Number of Cases	49	53
Total Number of Time Periods In Which Both Visual and IR Pictures are Available	144	135
Average Number of Time Periods Per Case	2.9	2.5

number of cases, the total number of time periods and the average number of time periods per case for both disturbance classes. At least 2 days of information is available for each case.

Data was selected from the years 1971-1975. The majority of cases for both disturbance classes come from the year 1972, an above average tropical cyclone year (see JTWC Annual Typhoon Report, 1972). During these years there were normally two DMSP satellites in polar orbit. They had daytime ascending nodes which were approximately 0800 and 1200 local time (LT). The Guam site would usually obtain two daylight and two night passes from each satellite. The night IR transparencies, although not used in the quantitative data composite, were used to track the individual disturbances to ensure continuity of systems. Table 2 gives the number of cases per year, the number of cases per 3 month interval, and the number of data samples occurring in the time intervals 0600-1000 LT and 1000-1400 LT for both disturbance classes.

The developing disturbances (ES1) are a data subset selected from a pre-tropical depression composite (Stage 1) established at Colorado

TABLE 2

Time Periods of the Developing and Non-developing Disturbaces

	Non-developing (00')	Developing (ES1)
Number of Cases per Year:		
1971	8	11
1972	38	26
1974	3	11
1975	0	5
Number of Cases per 3 Month Interval:		
JAN-MAR	0	3
APR-JUN	12	8
JUL-SEP	28	25
OCT-DEC	9	17
Distribution of Time Periods by Local Time:		
0600-1000 LT	95	84
1000-1400 LT	49	51

State University by Major Charles Arnold[2] (USAF) as part of a concurrent study (Arnold, 1977) of deep convection associated with various stages of tropical cyclone intensity. Only pictures that preceded his tropical depression stage by at least one day were chosen by the author to establish the developing (ES1) data set. Satellite data for each developing (ES1) case goes back as far as detectable by reasonable satellite tracing of each system's cloud patterns. The first data sample for each case precedes the first JTWC "best track"[3] position by an average of 3 days.

[2]Major Arnold established the DMSP site on Guam in 1971 and has an extensive background in satellite meteorology.

[3]Cyclone positioning based upon aircraft reconnaissance, satellite observations, land radar reports, and any other additional information which is formulated at the end of the typhoon season.

Only those disturbances which later reached at least tropical storm strength (maximum sustained surface winds of 34 to 63 knots) are retained in the ES1 data set.

In order to make meaningful comparisons with the developing (ES1) disturbance data set, a great deal of care and effort went into establishing the non-developing (00') disturbance data set. The author inspected approximately 1500 visual and 2000 infrared satellite transparencies to obtain a suitable sample of prominent non-developing cases. Only systems which appeared active in terms of penetrative convection and cirrus were chosen. Moreover, it was required that the non-developing disturbances be conservative to the extent that each remained convectively active for at least 24 hours. When the disturbance was detected, it was followed backward and forward in time until it could no longer be distinguished as being the same disturbance. Most non-developing disturbances chosen had lifetimes of 2-3 days and were tracked at velocities of 3-6^{o} per day. Nighttime IR tracking assured continuity.

2.2 Satellite data reduction

Figures 3 and 4 show eight visual and the corresponding IR pictures for 8 non-developing (00') and 8 developing (ES1) disturbances. The observed circle ($r \sim 83$ km) is centered on the best estimate by Charles Arnold of the forming or initial circulation center of the developing disturbances. Arnold selected disturbance centers primarily from the low-level cloud line arrangements and sometimes from cirrus outflow patterns. He has over 6 years of experience with DMSP satellite positioning procedures. His center position was based not only on

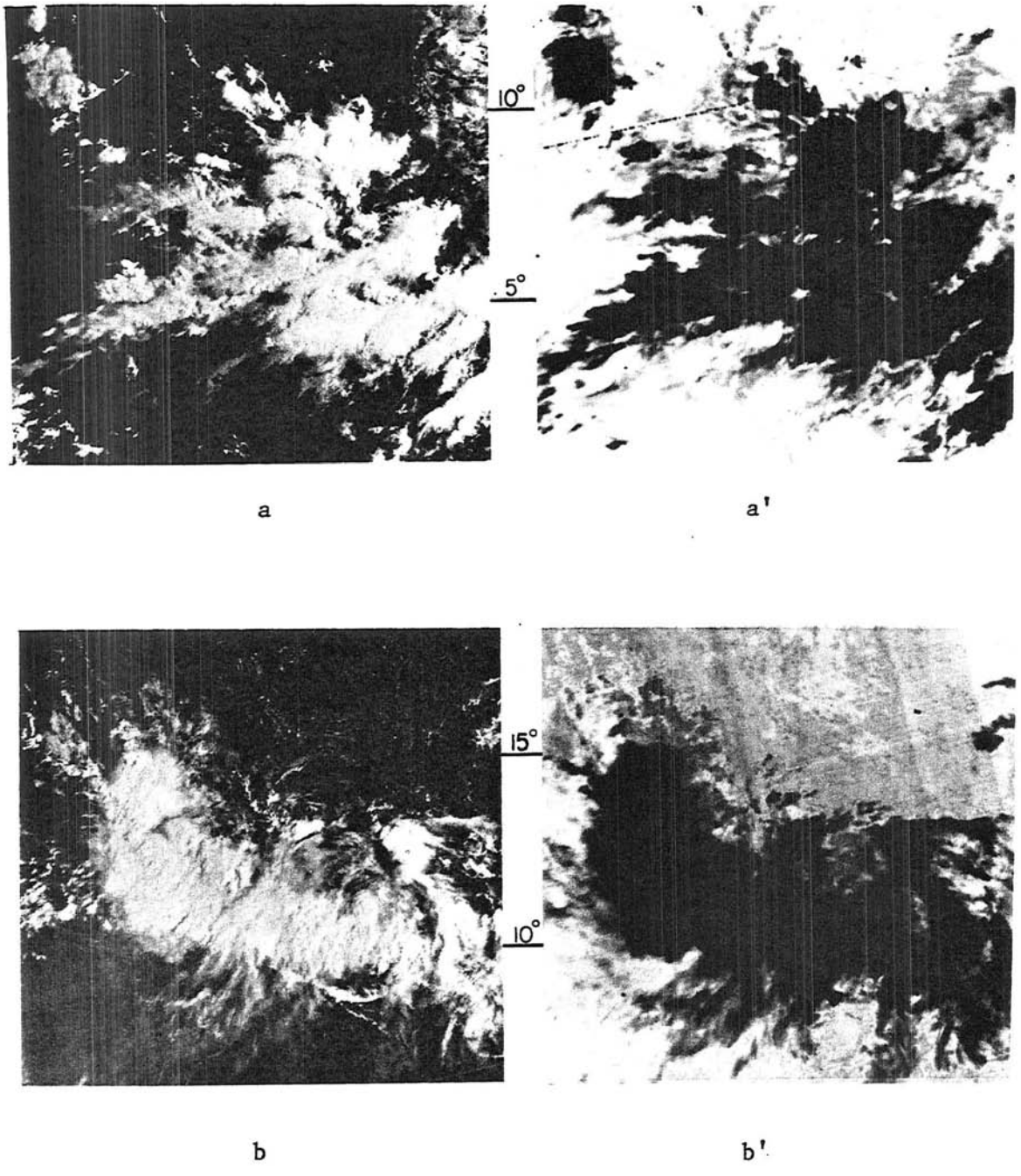

Fig. 3. DMSP satellite visual (a-h) and the corresponding infrared (a'-h') pictures of non-developing disturbances. The latitudes of each disturbance are indicated by the numbers between the pictures. The shading of the infrared pictures has been reversed. In contrast with the visual pictures, the darkest shade represents the highest cloudiness.

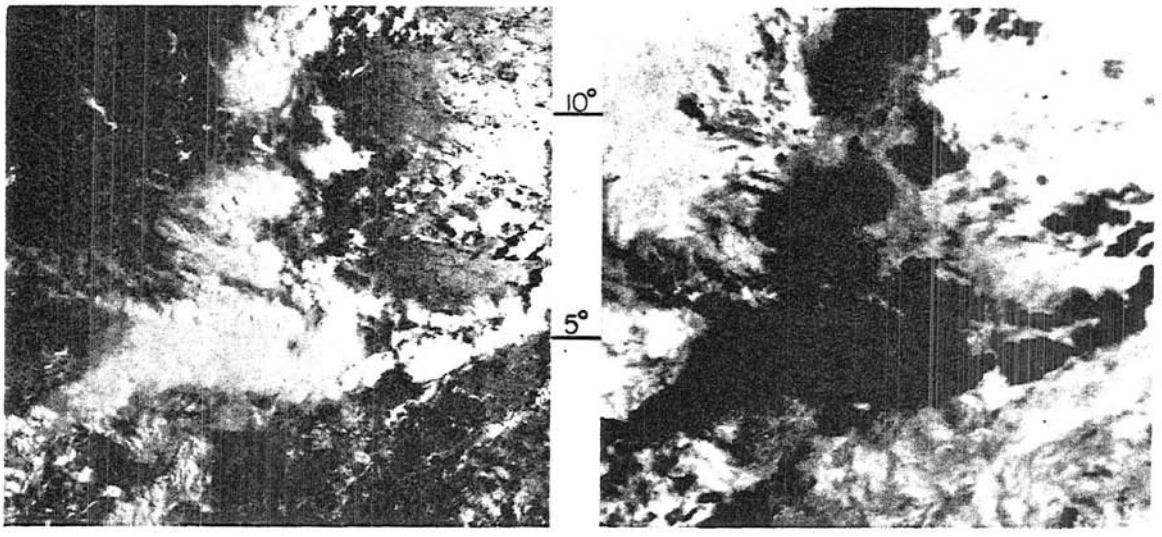

c c'

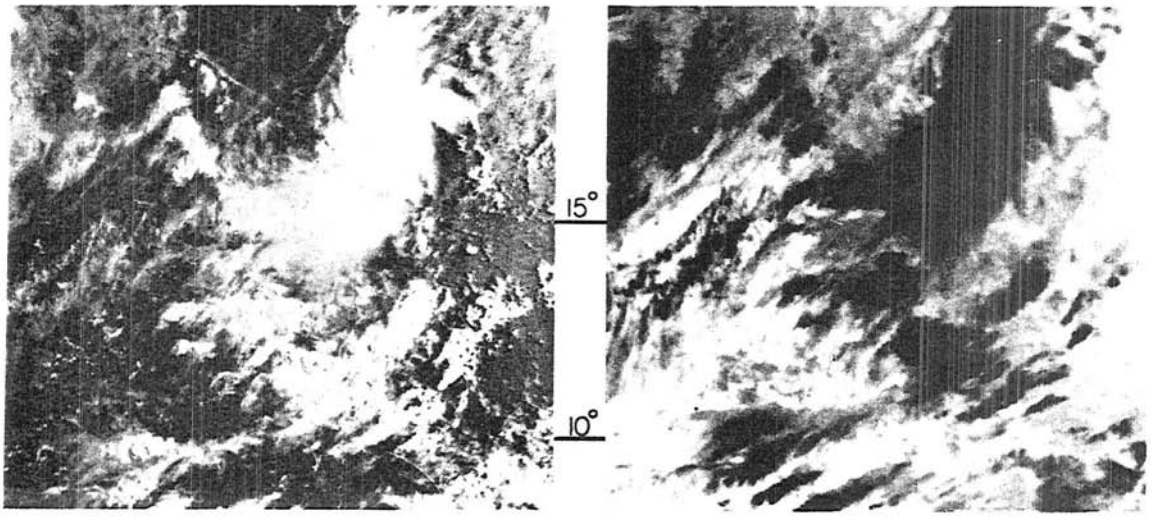

d d'

Fig. 3. Continued.

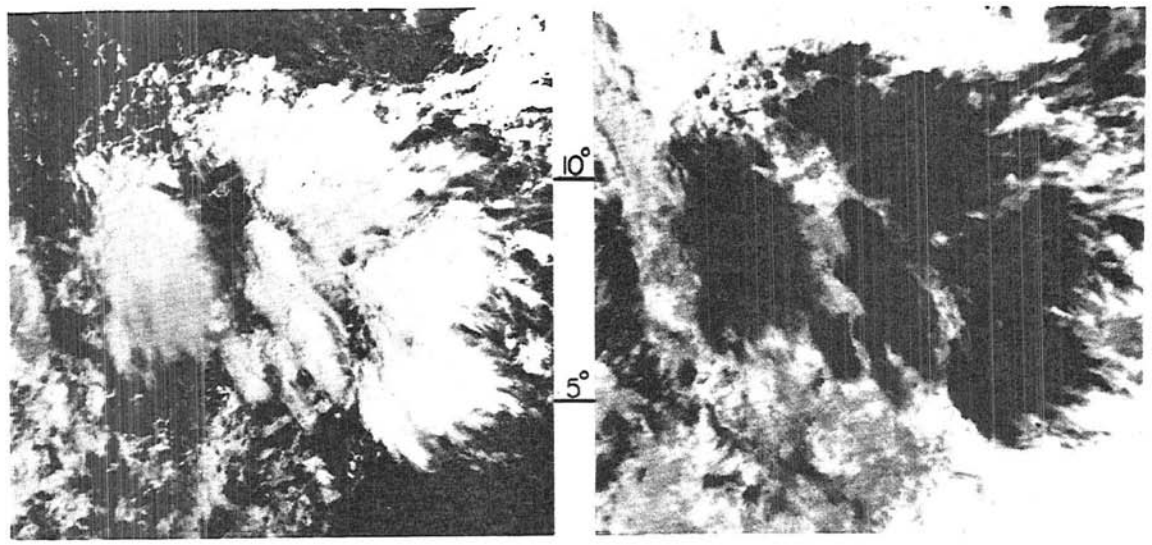

e e'

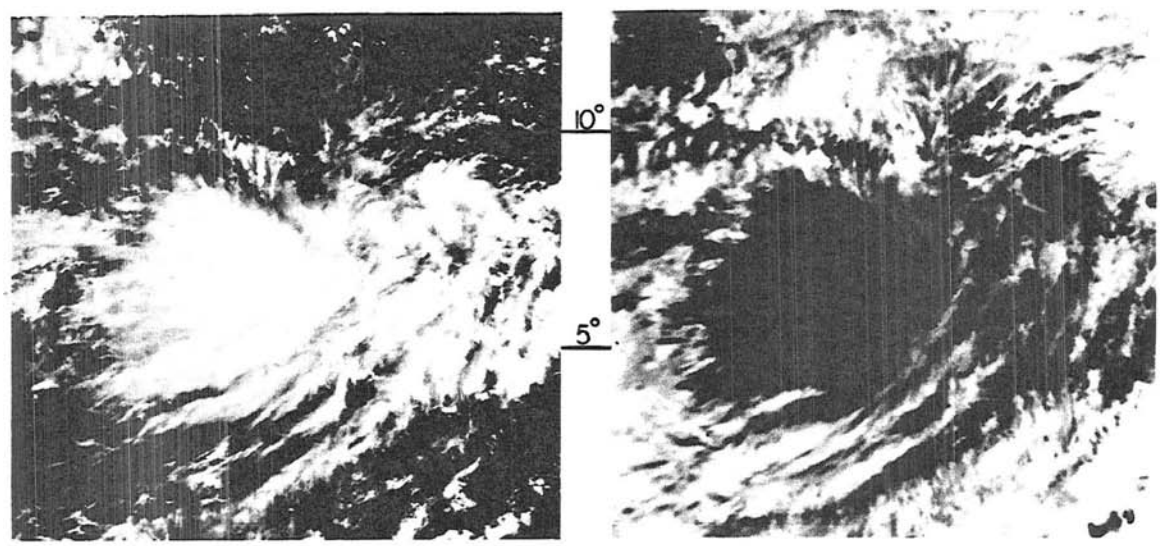

f f'

Fig. 3. Continued.

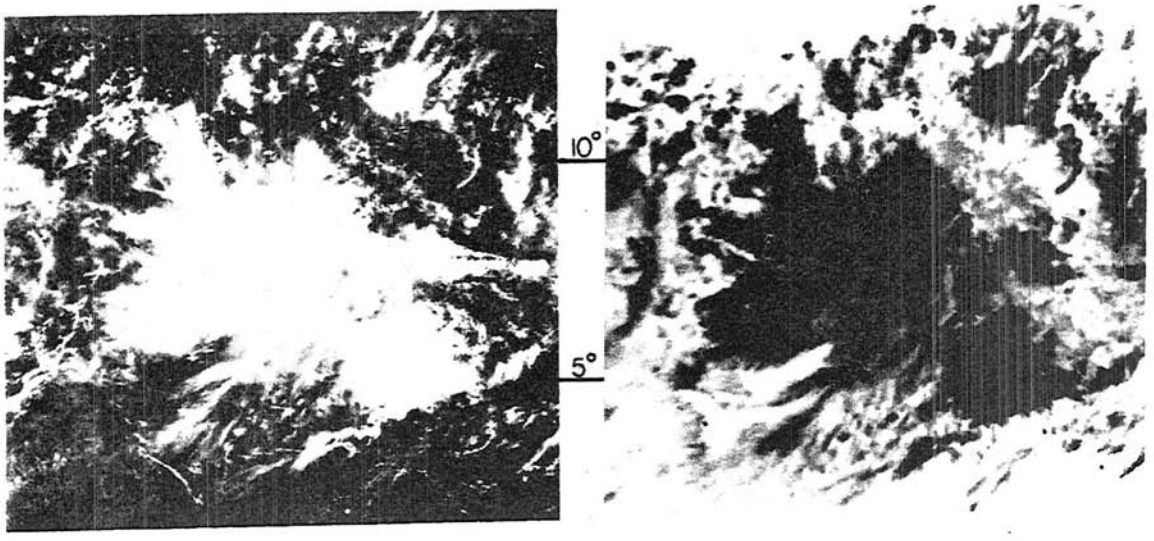

g g'

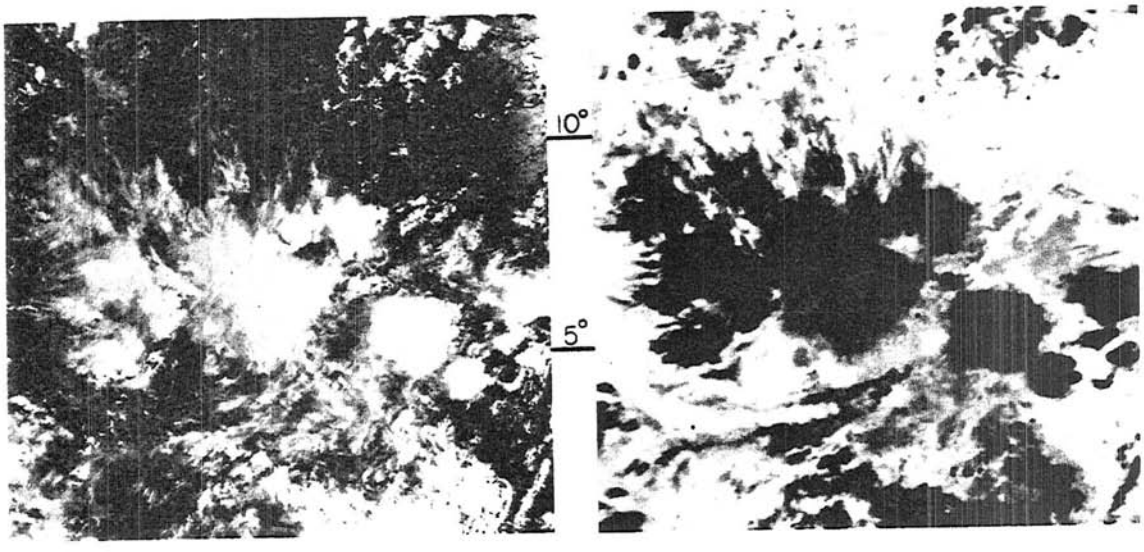

h h'

Fig. 3. Continued.

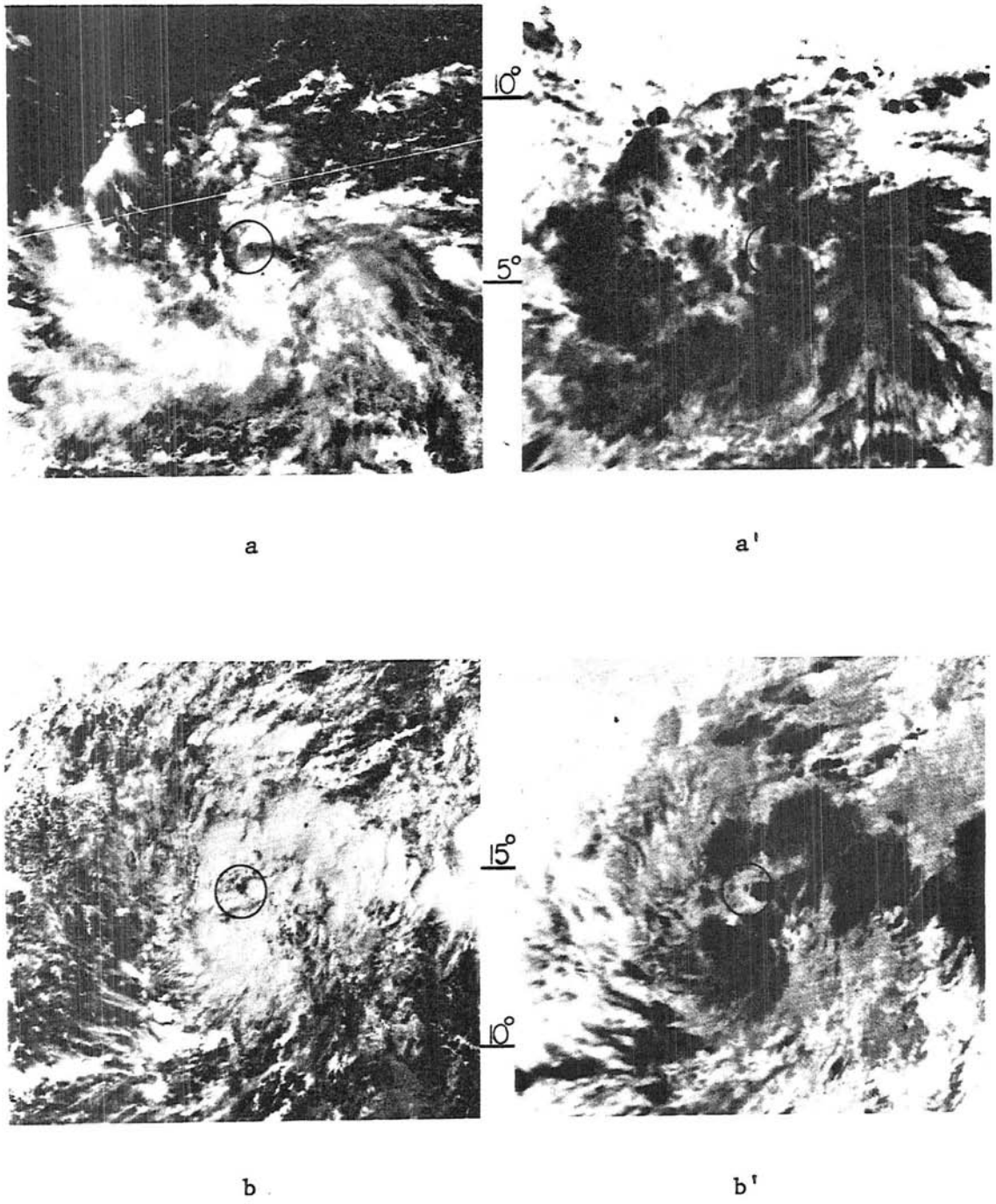

Fig. 4. DMSP satellite visual (a-h) and the corresponding infrared (a'-h') pictures of very early stage developing disturbances in which maximum sustained surface winds are less than 10-12 m s^{-1}. The circle (r ∿ 83 km) indicates where we believe the circulation of the forming or already formed cyclone is located.

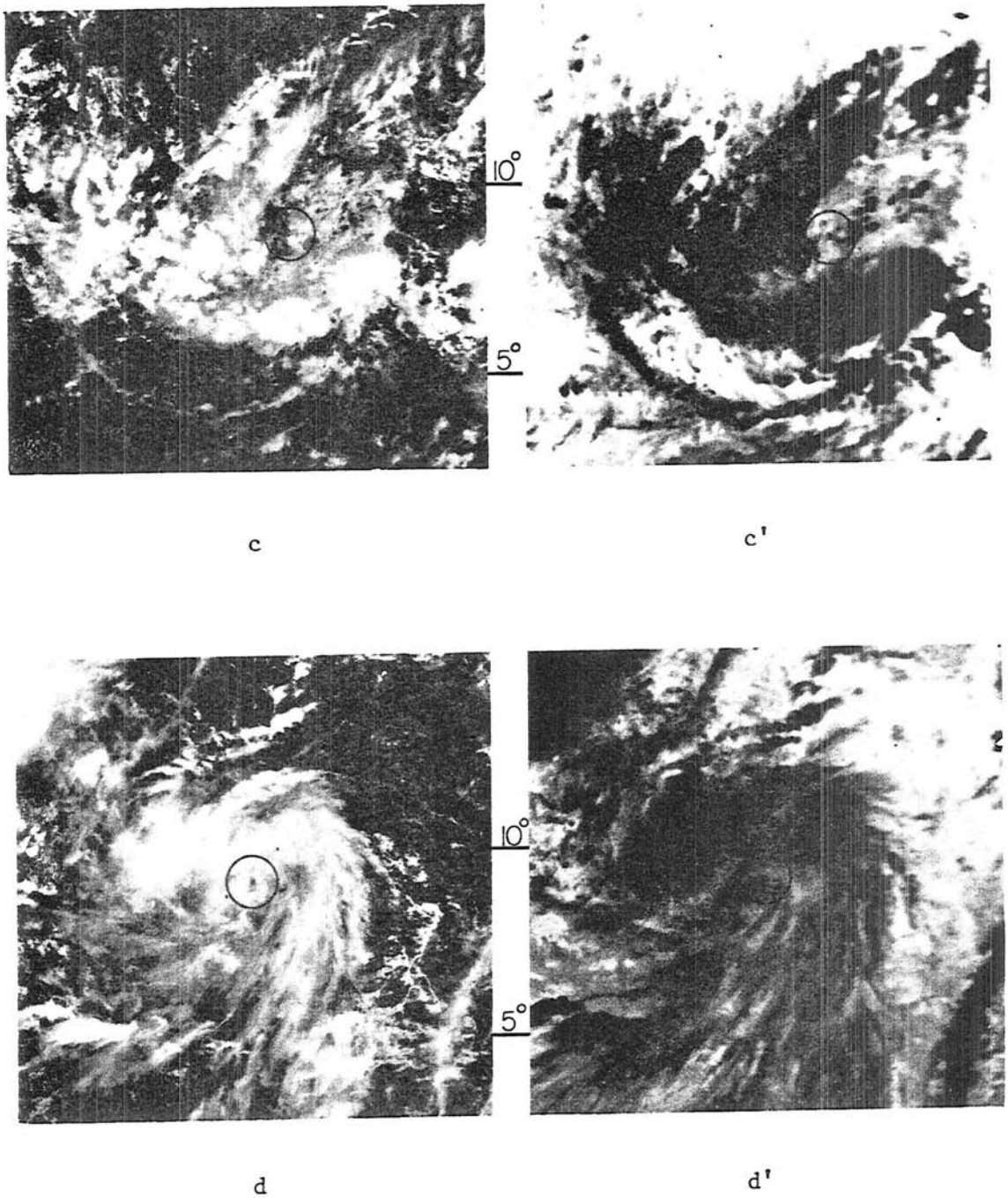

Fig. 4. Continued.

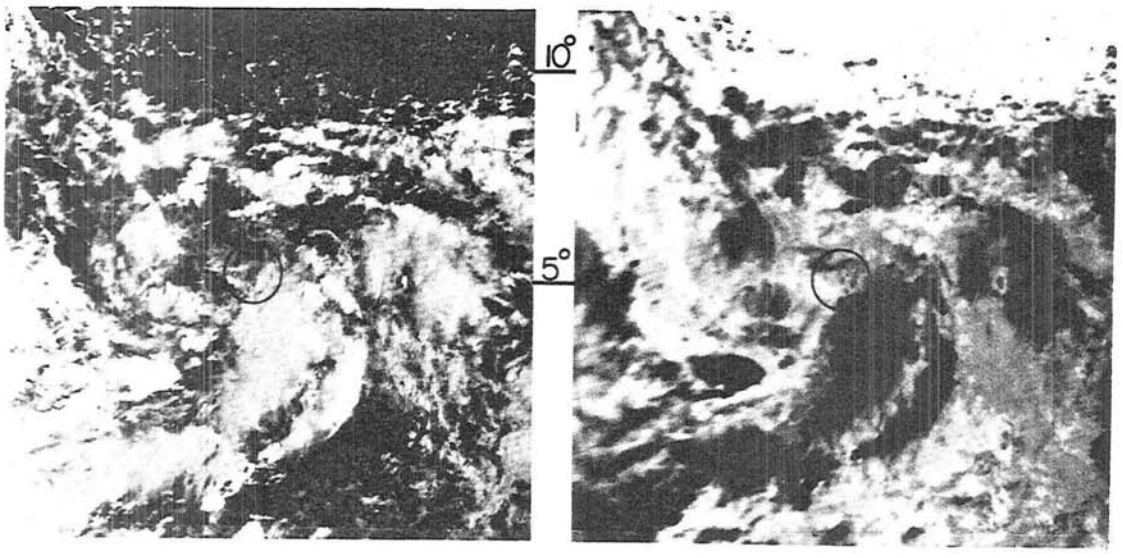

e e'

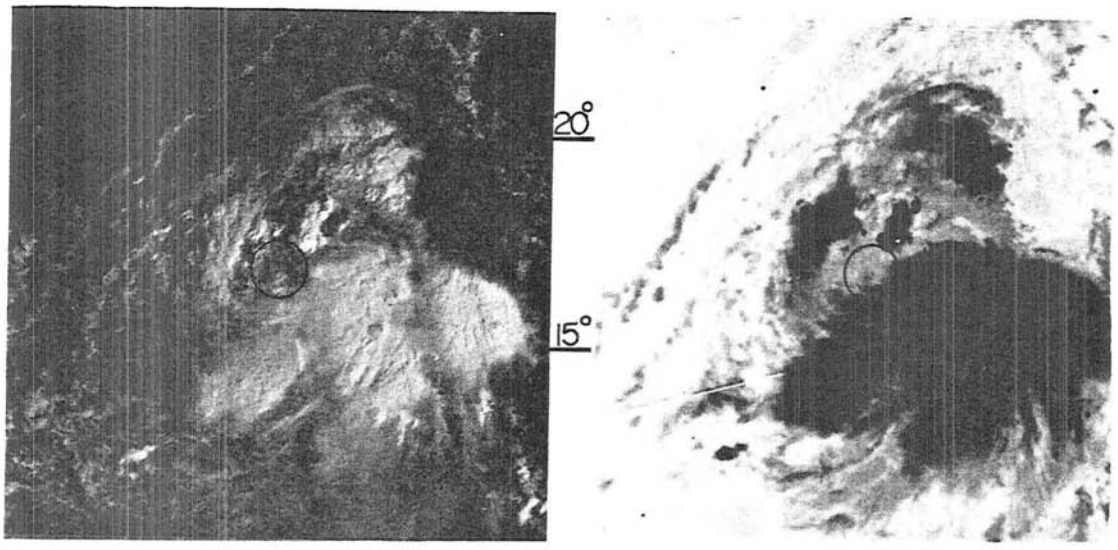

f f'

Fig. 4. Continued.

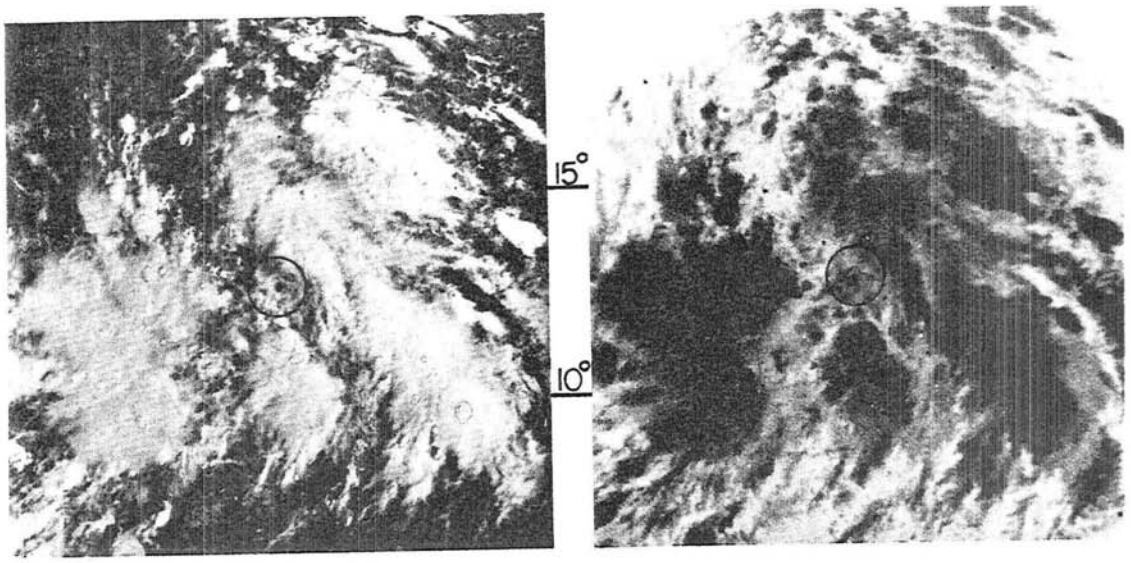

g g'

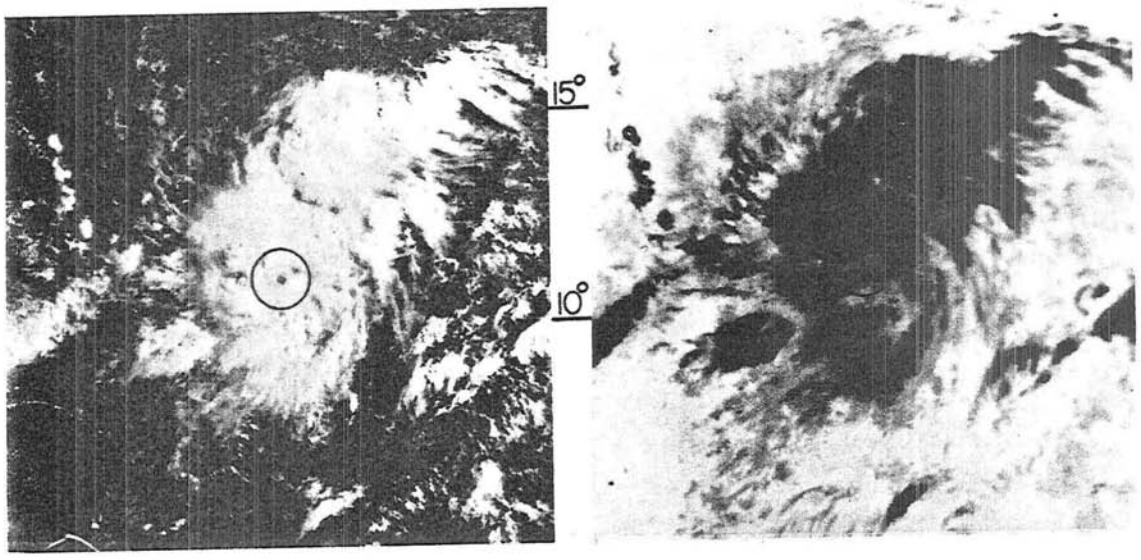

h h'

Fig. 4. Continued.

satellite observations, but also were from some aircraft investigative reconnaissance information. If the system circulation center could not be determined, the center of mass of the disturbance cloud clusters was taken as the disturbance center. Seventy-five percent of all developing disturbances had circulation centers defined by visible low-level curved cumulus lines within the clear region surrounding the disturbance or by semi-cloud free regions within the disturbance periphery. Of these, 25% occurred on the side of or in the cradle position of the disturbance (see Fig. 4g for example), and 50% occurred entirely within the disturbance (see Fig. 4d) but typically between deep convective elements. In the remaining 25% of cases, the center of mass was used to define the disturbance center. For a more detailed discussion on tropical cyclone positioning, the reader is referred to 1st Weather Wing Pamphlet 105-10 (Arnold, 1974). The visible circulation center and its implications for cyclone genesis will be discussed later.

A circulation center was usually not visible in the non-developing disturbances, and no additional early investigative information was available. In these cases the system's center was taken to be the center of mass of the disturbance cloud clusters.

Area measurements of penetrative convection and cirrus were made on the CSU Optical Data Digitizer and Display System (see Appendix B) utilizing a technique developed by Arnold (1977). Measurements were made in each disturbance class for the following 3 data sets:

1) Cb convective elements that were digitized according to albedo brightness from the visual transparencies,

2) Cb convective elements that were hand traced from the visual transparencies, and

3) Cirrus cloud amounts classified according to the coldest three shades ($\sim 6^{o}$ Kelvin resolution) of IR temperature.

The overlay grid used in the analysis is shown in Fig. 5. The grid, consisting of 25 rectangular sections (5x5 area), was originally designed for data set 1. The dimensions of each section (316 x 296 km in x-y coordinates) were specified such that the 512 x 480 pixel or element representation on the OD^3 system gave a geometric resolution comparable to the .33 n mi (.62 km) visual satellite transparency. The grid was further stratified according to a 3x3 area ($r \sim 4.2^{o}$ latitude), a 1x1 area ($r \sim 1.4^{o}$ latitude) and 2 outer radius areas referred to as Outer 8 and Outer 16.

Area measurements of deep convection for data set 1 were determined from digitized pixel or element values based upon a specified density or albedo range (see Appendix B). The density range was determined by the OD^3 system as part of a brightness set-up for each new transparency. Deep convection, if present, was digitized in each of the 25 rectangular sections and stored on magnetic tape. The percent area covered by deep convection was later computed and stratified by a CDC 6400 computer for each of the rectangular sections and the various grid areas shown in Fig. 5. By making use of all 25 sections, disturbances which were partially off the transparency could be used in evaluating convection for the average or composited disturbance by applying a normalization factor.

In data set 2, convective elements that were clearly penetrating the cirrus canopies were outlined and darkened in on tracing paper for each disturbance within the 5x5 area ($r \sim 7.1$). The area of these convective elements was then measured by the OD^3 system within the 5x5,

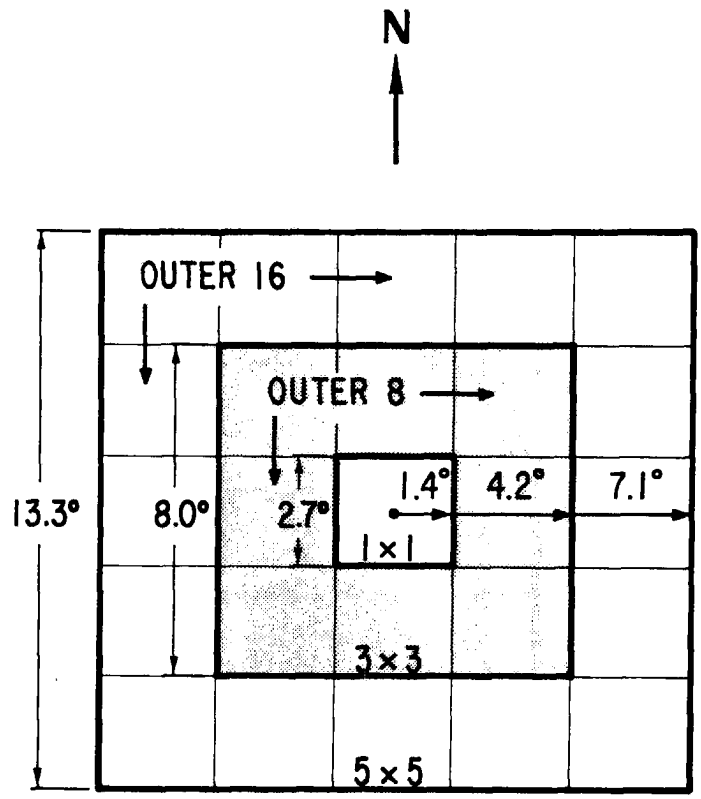

Fig. 5. Overlay grid used to make measurements of penetrative convection and cirrus from the satellite data. The grid was oriented to the north and was centered on the disturbance. Measurements could be made within each rectangular section, the 5x5 area ($r \sim 7.1^{o}$ degrees latitude), the 3x3 area ($r \sim 4.2^{o}$) or the 1x1 area ($r \sim 1.4^{o}$). Outer 16 = (5x5 area) - (3x3 area) and Outer 8 = (3x3 area) - (1x1 area).

3x3 and 1x1 grid areas and directly printed out. The number of data samples in each disturbance class was reduced somewhat since measurements were not made in each of the 25 rectangular sections for all systems.

Infrared transparencies, which directly correspond to the visual data used for tracing, were used in the cirrus analysis. The top 3 gray shades in the IR data were digitized and measured by the OD^{3} system within the same grid areas defined for the second data set. The infrared sensor has a 100^{o} Kelvin detection range (210-310 K) which is converted into 16 gray shades on the transparency. Clouds colder than

210 K are grouped in one category. The top 3 gray shades correspond to temperatures of: $\leq$ 210 K, 211 - $\leq$ 216 K, and 217 - $\leq$ 222 K. This temperature range effectively specifies the amount of cirrus. The lighter two cirrus shades correspond to thin cirrus, since some long wave radiation from below affects these measurements. The coldest shade of IR corresponds to thick cirrus produced by current or very recent Cb convection.

2.3 Rawinsonde data reduction

As indicated earlier, DMSP satellite coverage over the area of interest was such that usually four visual and four IR pictures were available per day within 4 hours of 00Z (10 LT). Thus, a very accurate 00Z disturbance position for the rawinsonde analysis was determined. The 12Z disturbance position was determined by interpolating between the two 00Z positions. A total of 66 and 134 rawinsonde soundings were available within 5^{o} radius of the centers of developing and non-developing disturbances, respectively.

The rawinsonde compositing philosophy and technique are described in detail in works by Zehr (1976), Williams and Gray (1973), Ruprecht and Gray (1976), George and Gray (1976) and Frank (1976), and will not be reiterated here. These studies were always based upon large data samples, which is an underlying assumption of the technique. It was, therefore, an interesting experiment to try this technique on a smaller data sample. The only time periods used were those in which the disturbance position was assured. The unique high resolution DMSP data made this possible.

The same grid used by Zehr (1976) was utilized in this study (see Fig. 6). The center of the grid was centered on the disturbance center and rawinsonde soundings were composited within the grid. The average dynamic and thermodynamic parameters were then determined from the composited soundings. Computations were made in a stationary coordinate system.

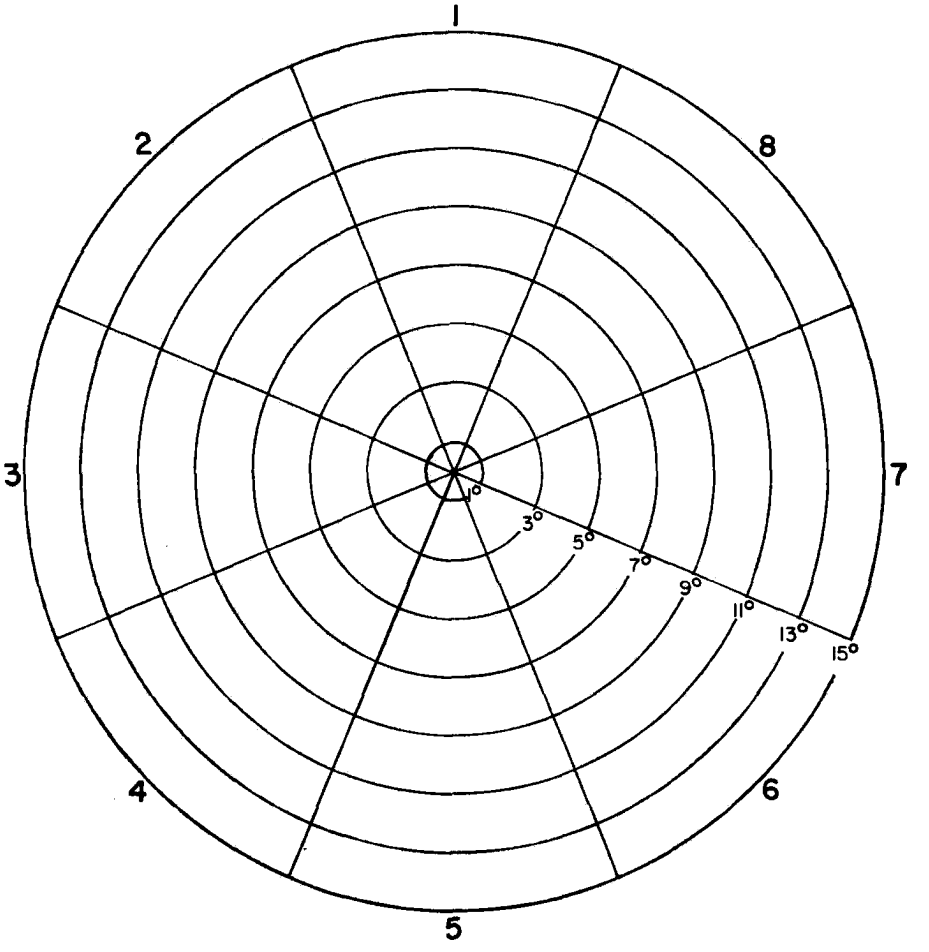

Fig. 6. Grid used to composite rawinsonde data (from Zehr, 1976). The grid consists of 8 octants and 8 radial bands, so that observations were averaged in each grid resulting in an 8x8 array of values. The grid was centered on the disturbance center with octant 1 oriented to the north (1^{o} latitude/longitude = 111 km).

3. SATELLITE COMPARISON OF DEVELOPING AND NON-DEVELOPING DISTURBANCES

A better understanding of the physical processes and an aid to forecasting of cyclone genesis might be attained by comparing developing disturbances with similarly appearing non-developing disturbances of the same location, season and thermodynamic conditions. Typical examples of both disturbance classes have been shown in Figs. 3 and 4. Physical characteristics and quantitative area measurements of Cb convection and cirrus are given below.

3.1 Physical characteristics

As the data sets were being established, physical characteristics for each disturbance class were determined and are documented in Table 3.

The most notable difference between these disturbance classes is the upper-level (cirrus) flow pattern. When cirrus streaks are clearly visible, wind vectors corresponding to cirrus diverging away from the deep convective elements can be drawn on the visual satellite transparencies. The general disturbance cirrus level outflow characteristics can then be determined from a qualitative analysis of these cirrus vector streaks. Approximately three times as many developing disturbances were observed to have upper-level anticyclonic outflow than did non-developing systems. A representative sample of the wind vectors drawn for the two disturbance classes (ES1 and OO') and a comparison with Zehr's (1976) 200 mb rawinsonde outflow wind vectors from his developing and non-developing disturbances are given in Chapter 4. Satellite and rawinsonde winds compared quite well.

TABLE 3

Mean Physical Characteristics of Developing (ES1) and Non-developing (00') Disturbances

Physical Characteristic	Non-developing (00')	Developing (ES1)
Average Lifetime (days)	2.0	3.4*
Minimum-Maximum (days)	1-5	2.5-5.5*
Average Total Life of Storm (days)	N/A	9.5
Average Speed of Movement ($m\ s^{-1}$)	6.4	5.1
Shape (% of total cases):		
Elliptical	29.7	33.3
Wave	5.4	20.0
Circular	33.8	15.5
Irregular	31.1	31.2
Average Size (degrees radius):		
North Radius	3.5	4.0
East Radius	4.6	5.1
South Radius	3.7	4.2
West Radius	4.0	4.2
Average Radius	3.9	4.4
Average Direction Disturbance Moving to	275°	290°
Qualitative Judgement of Amount of Deep Convection(% of total cases) Classified as:		
Light	28.5	28.1
Moderate	47.9	47.8
Intense	23.6	24.1
Anticyclone Visible at Cirrus Level (% of total cases)	20.7	63.8

*Average based upon Arnold's (1977) entire pre-tropical depression stage.

The average size of each disturbance was determined by assigning a numerical radius value (degrees latitude) to the cloud extent measured from the center of the system in the four cardinal directions (see Fig. 7). It is obvious that this measurement can be somewhat misleading at times, since the assigned radius is not representative of overall cloudiness but rather a measure of the extent of apparent total disturbance cloudiness which also includes some areas of obvious subsidence and minimum convection. The average size of the developing disturbance is larger than the non-developing disturbance by an average of $\sim$ 15% or 1^{o} in diameter.

In general, most non-developing disturbances have short lifetimes of 2-3 days or less. Many prominent cloud systems of disturbance size last for a period of less than 24 hours. Our non-developing systems were chosen only if their lifetimes were greater than 1 day. Implications are that tropical disturbances of this type in western North Pacific regions that have the potential to maintain themselves for more than two days will likely intensify into tropical cyclones.

3.2 Quantitative comparison of penetrative convection and cirrus

As indicated earlier, the non-developing (00') and developing (ES1) disturbances of this study are very comparable (see Tables 1 and 2 and Fig. 2). Great care was taken to process all the data in the same manner. Measured values of cirrus and convection, although perhaps not precisely accurate at each time period, are certainly representative in the statistical and comparative sense.

The overall size of the average disturbance (see Table 3) is approximately 4^{o} in radius. Therefore, the 3x3 area ($r \sim 4.2^{o}$) is most representative of the cloud part of the disturbance. Measurements

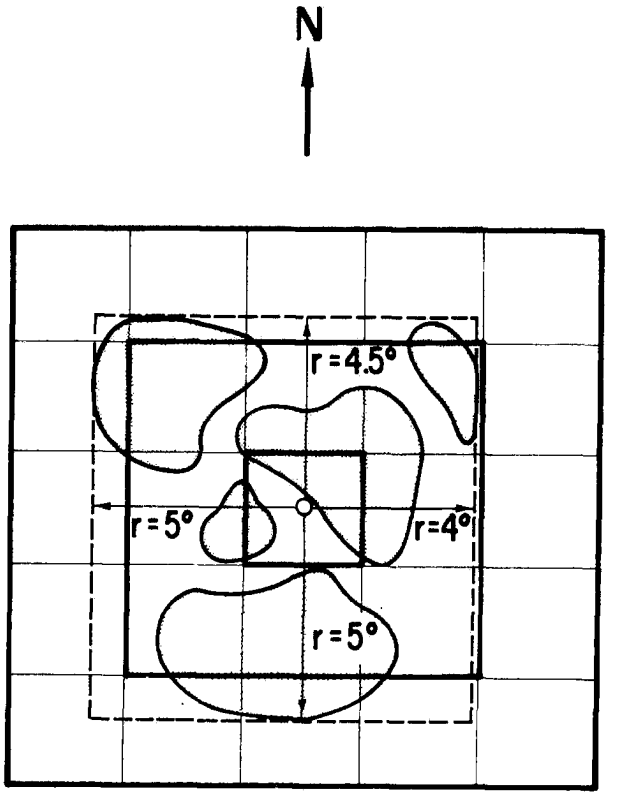

Fig. 7. A typical disturbance example and the overlay grid. A quantitative radial measurement defined by the cloud extent considered to be part of the disturbance was assigned in each of the 4 cardinal directions. The average radius of this disturbance is 4.6°.

beyond the 3x3 area are more representative of the surrounding environment (typically a variable cloud region). Outer radius determinations were made by subtracting out inner grid areas. These are identified as Outer 8, and Outer 16, determined by:

$$\text{Outer 8 (\% area coverage)} = \frac{(9)\ X\ (\%\ 3x3) - (\%\ 1x1)}{8} \quad \text{and}$$

$$\text{Outer 16 (\% area coverage)} = \frac{(25)\ X\ (\%\ 5x5) - (9)\ X\ (\%\ 3x3)}{16}$$

where % is the percent area covered by penetrative convection or cirrus within those specified grid areas.

Convection. Penetrative convection is defined as deep convection which can be viewed by satellites either standing by itself or visible above the cirrus shield. The quantitative area measurements of convection obtained from both data processing techniques (digitized, traced) are presented in Table 4. Figure 8 shows two examples of traced convective elements for the developing and non-developing disturbances.

As one would expect, the percent area covered by penetrative convection is small and decreases rapidly beyond the inner 1x1 area. Malkus et al. (1961) determined the percent area covered by penetrative convection in Hurricane Daisy (1958) to be $\sim$ 4% within 200 n mi of the storm center. This is in some agreement with the results presented in Table 4 within the 3x3 ($r \sim 4.2^{o}$) area. In general, the results obtained independently by two different techniques support one another. Magnitudes of convection are somewhat different, but the general decrease of convection from inner to outer radius is similar. The author believes the best penetrative convection results were those obtained by the tracing technique. No significant differences in penetrative convection appear to exist between the two systems. The primary differences occur at outer radii or in the surrounding environment. The most important difference appears to be not in the percent area covered by penetrative convection, but rather the way in which the convection is distributed.

The average penetrative convective element diameter (km) and number of these elements for various grid stratifications are indicated in Table 5. The average size of the convective elements is very large ($\sim$ 26-34 km in diameter). It is obvious that multiple deep convective

TABLE 4

Penetrative Convection Area Coverage (Percent)

Disturbance Class	Grid Stratification				
	1x1 r∿1.4°	3x3 r∿4.2°	5x5 r∿7.1°	Outer 8 r∿1.4-4.2°	Outer 16 r∿4.2-7.1°
Data Set 1 (Digitized)					
Non-developing (00') Sample size (144)	4.9	3.3	2.9	3.1	2.6
Developing (ES1) Sample size (135)	4.8	3.7	3.3	3.6	3.1
Data Set 2 (Traced)					
Non-developing (00') Sample size (102)	6.0	2.4	1.1	2.0	.3
Developing (ES1) Sample size (92)	5.7	3.0	1.8	2.7	1.1

TABLE 5

Penetrative Basic Convective Element Number and Average Size Distribution Based on Data Set 2 (Traced)

Disturbance Class	Grid Stratification				
	1x1 r∿1.4°	3x3 r∿4.2°	5x5 r∿7.1°	Outer 8 r∿1.4-4.2°	Outer 16 r∿4.2-7.1
Non-developing (00')					
Average Number	8	32	40	24	8
Average BCE Diameter (km)	30	28	28	28	26
Developing (ES1)					
Average Number	7	33	50	26	17
Average BCE Diameter (km)	32	32	32	32	34

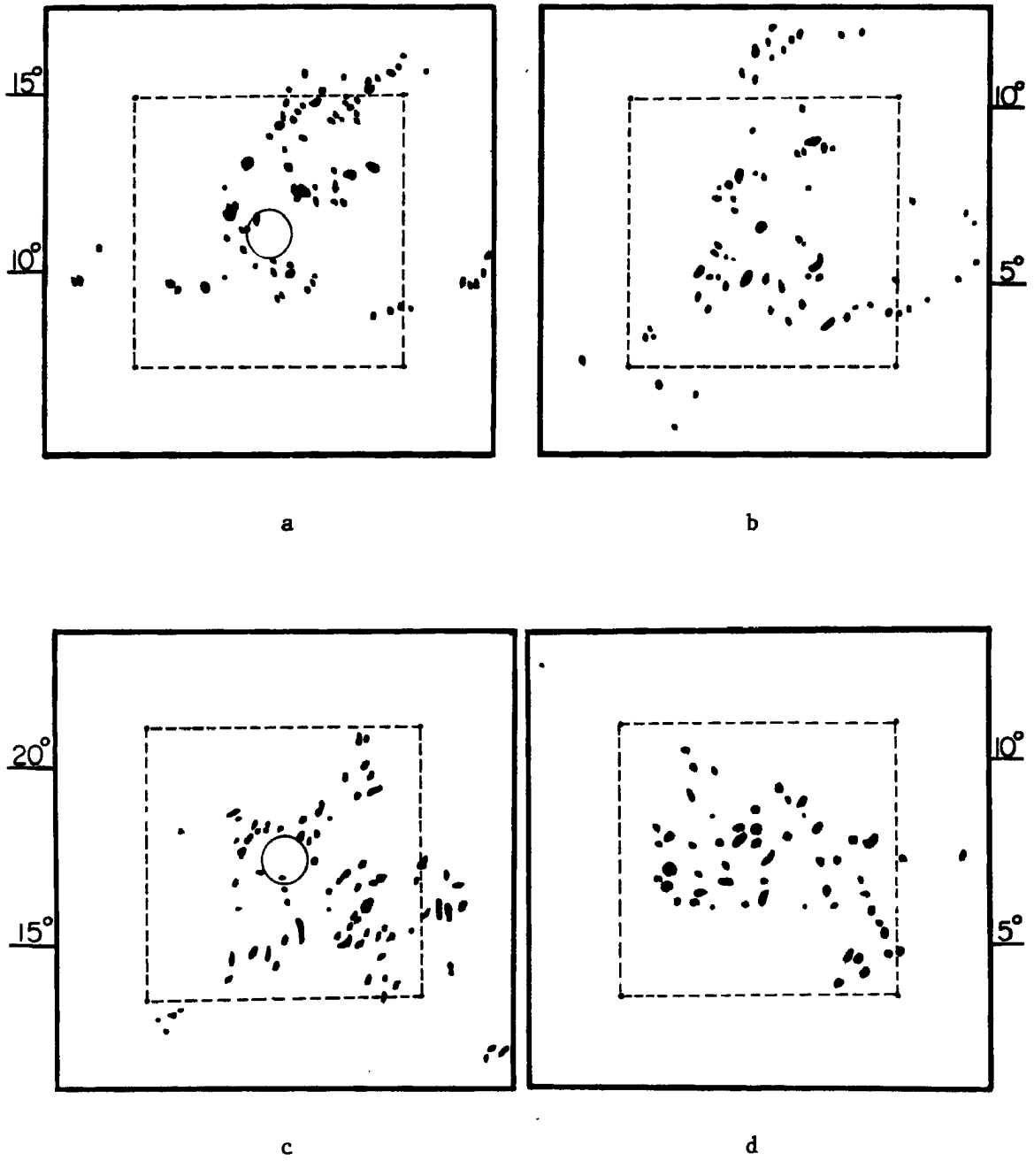

Fig. 8. Typical example of traced penetrative convection for two developing (a and c correspond to Figs. 4h and 4f, respectively) and two non-developing (b and d correspond to Figs. 3c and 3g, respectively) disturbances within the 5x5 area.

cell complexes made up of up-and-downdraft cells were usually measured. Arnold (1977) has described these cell groups as "Basic Convective Elements" (BCE). The reader is referred to his paper for a discussion on the physical meaning of these basic convective elements. The basic convective element size is approximately the same between disturbance classes except in the Outer 16 or environmental region (see Table 5). The author feels this is a result of the greater amount of total cirrus observed in the developing disturbance composite at outer radius. Increased amounts of cirrus make it more difficult to distinguish between the basic convective elements and the cirrus in which they are often embedded. Their size is sometimes hard to measure. Basic convective element number distribution is about the same between disturbance classes except in the Outer 16 region. The average developing disturbance apparently exists in a more favorable moisture environment. The basic convective element number and their distribution according to quadrant are given in Table 6. The eastern and southern half of the average developing disturbance shows the greatest concentration. Convection is more uniformly distributed in the average non-developing disturbance which is consistent with the choice of the center of mass as the disturbance center.

Cirrus. Cirrus canopies originate from deep cumulonimbus clouds as they penetrate the upper tropospheric stable layers ($\sim$ 200-150 mb). The visual appearance of cirrus appears to depend upon upper-level wind patterns and the way in which the deep convection is distributed within the disturbance. The IR data best shows the cirrus thickness differences over each disturbance (see Figs. 3 and 4). The top three gray shades on the IR data represent the total cirrus of the

TABLE 6

Penetrative Basic Convection Element Distribution Based on Data Set 2 (Traced) by Quadrant Within the 5x5 Area ($r \sim 7.1^{o}$)

Disturbance Class	Grid Stratification			
	Northeast $0\text{-}90^{o}$	Southeast $90\text{-}180^{o}$	Southwest $180\text{-}270^{o}$	Northwest $270\text{-}0^{o}$
Non-developing (00') Average Number	11	10	10	9
Developing (ES1) Average Number	14	15	13	8

weather disturbance and are the values presented in this section. Total cirrus is an approximate measure of the mean vertical motion occurring in the disturbance. Interpretation of the individual shades that determine the total cirrus is more difficult.

Table 7 presents the results of the cirrus measurements. Total cirrus ($T \leq 222$ K) values support the penetrative convection measurements. No significant difference is noted except at outer radius. This is a reflection of the lack of deep convection differences between disturbance classes except in the Outer 16 area. Only slightly more upper-level divergence was observed to exist at outer radius in the average developing disturbance (see section 4.2).

The more interesting measurements are indicated in the individual cirrus gray shades. There is a higher percentage of area covered by cirrus I (coldest) in the non-developing composite at all radii. The non-developing disturbance is observed to have 40% more top shade cirrus within the 1xl area. This appears to be the result of a few ($\sim$ 25%) of

TABLE 7

Cirrus Area Coverage (Percent) for Data Set 3

Disturbance Class	Grid Stratification				
	1x1 r∿1.4°	3x3 r∿4.2°	5x5 r∿7.1°	Outer 8 r∿1.4-4.2°	Outer 16 r∿4.2-7.1°
Cirrus I (T≤210 K)					
Non-developing (00')	43	20	9	17	5
Developing (ES1)	31	16	9	14	4
Cirrus II (210 K<T≤216 K)					
Non-developing (00')	23	15	8	14	4
Developing (ES1)	29	20	13	19	9
Cirrus III (216 K<T≤222 K)					
Non-developing (00')	10	11	7	11	5
Developing (ES1)	15	14	12	14	11
Total Cirrus (T≤222 K)					
Non-developing (00')	76	46	24	42	14
Developing (ES1)	75	50	34	47	24

the developing disturbance centers being chosen on the edge of the system's cloudiness. Cirrus also tended to blow across the disturbance center unidirectionally (Dvorak, 1975) in the non-developing cases causing an accumulation of cirrus. Cirrus may also tend to accumulate in the non-developing system due to a smaller percentage of outer radius convection and slightly weaker cirrus level divergence. By contrast, there is a higher percentage of area covered by the reamining two cirrus shades (thin cirrus) in the developing disturbance composite at all radii. Enhanced outer radius convection and a tendency for cirrus level anticyclonic flow at outer radius (i.e., $r > 2^{\circ}$) are processes which likely thin the cirrus out more rapidly in the average early developing disturbance.

Summary. The DMSP satellite observed cloud characteristics between these two classes of systems which are worth noting are:

1) The percent area covered by penetrative convection and total cirrus within the 1x1 area ($r \sim 1.4^{o}$) and the 3x3 area ($r \sim 4.2^{o}$) is much the same.

2) There is significantly more penetrative convection ($\sim$ 3 to 1) and total cirrus ($\sim$ 2 to 1) in the outer environmental area of the developing disturbances. These systems are more distinguished by their convective differences at outer radius.

3) Cirrus density (three IR gray shades) differences between disturbance classes indicate cirrus level outflow patterns to be significantly different between systems. In general, flow is anticyclonic in the developing disturbance and unidirectional in the non-developing disturbance.

4) The average lifetime of even the more conservative non-developing disturbances is short. Disturbances that have the potential to maintain themselves for more than two days have a significantly higher intensification potential.

These differences might prove to be useful as forecasting aids.

4. RAWINSONDE COMPARISON OF DEVELOPING AND NON-DEVELOPING DISTURBANCES

For quantitative information the compositing or averaging of rawinsondes must be used over data sparse regions (see Fig. 2). The mean dynamic and thermodynamic parameters of the composited disturbance and surrounding environment are determined from a sufficiently large number of soundings which are specified by individual disturbance positions at 00Z and 12Z. If the characteristics of the two disturbance systems are significantly different then the physical process between the two systems can likely be determined.

The dynamic and thermodynamic parameters used are given in Table 8. Divergence, mean vertical motion and relative vorticity were evaluated for various radial areas in cylindrical coordinates from the radial and tangential winds in composite form.

Data selection and location for this study are very comparable to Zehr's (1976) developing (Stage 2)[4] and non-developing (Stage 00) disturbances. Mean vertical motion ($r = 0\text{-}4^{o}$), relative vorticity ($r = 0\text{-}4^{o}$), and 200 mb wind data from the Zehr (1976) developing (Stage 2) and non-developing (Stage 00) rawinsonde composites are shown for comparison.

4.1 Mean thermodynamic differences

Table 9 shows the computed differences in geopotential height (Z), temperature (T), relative humidity (RH), and specific humidity (q) between the disturbance classes. In general, these differences are

[4]Developing disturbance rawinsonde composite which included all time periods prior to the time the disturbances reached sustained winds of 15 m s^{-1}.

TABLE 8

Dynamic and Thermodynamic Parameters

DYNAMIC

u	=	East-west component of wind
v	=	North-south component of wind
V_R	=	Radial wind
V_T	=	Tangential wind

THERMODYNAMIC

Z	=	Geopotential height
T	=	Temperature
RH	=	Relative humidity
q	=	Water vapor mixing ratio

TABLE 9

Thermodynamic Differences for r = 0-3° (ES1 minus 00')

P (mb)	Z (meters)	T (°C)	RH (%)	q (g k gm^{-1})
100	2.0	-.3		
150	10.9	.4		
200	8.6	.4		
250	6.9	.3		
300	5.8	.4		
400	.9	.4		
500	-2.1	.5	6.0	-.1
600	-5.4	.3	-.4	-.3
700	-5.1	-.2	3.9	-.2
800	-4.9	.2	.2	-.4
850	-5.0	-.2	-2.2	.1
900	-4.6	-.3	-.5	-.1
950	-4.5	-.3	-.7	.1
1000	-6.1	-.4	-.9	-.3

observed to be small and insignificant. They indicate that the average developing disturbance is at an early stage of development and thermodynamically differs little from the non-developing disturbance. The disturbance ($r = 0\text{-}3^{o}$) to environment ($r = 3\text{-}7^{o}$) gradients of moisture and temperature are shown in Figs. 9 and 10, respectively. The largest difference is apparent in the moisture profile where the developing disturbance has a more favorable moisture environment by 0.5 to 1.0 gm kg^{-1}. This supports the satellite composited results which indicated more convection at outer radius in the developing disturbances.

4.2 Divergence and vertical motion

Profiles of divergence, computed from the mass balanced radial winds (V_R) for $r = 0\text{-}4^{o}$ and $r = 0\text{-}6^{o}$, are shown in Figs. 11 and 12, respectively. A deep layer of convergence (surface to 400 mb) and a maximum outflow layer at 200 mb are observed in both disturbance classes. The differences over $r = 0\text{-}4^{o}$ and $r = 0\text{-}6^{o}$ between the average developing and non-developing disturbances are, in general, small.

The corresponding mean vertical motion profiles, derived kinematically from the radial winds, are shown in Figs. 13 and 14. In addition, mean vertical motion over $r = 0\text{-}4^{o}$ from the Zehr (1976) developing (Stage 2) and non-developing (Stage 00) disturbances are shown in Fig. 15 for comparison. The maximum mean vertical motion ($\sim$ 400 mb) in the average developing (ES1) disturbance is observed to be larger than the non-developing (00') disturbance by about one-third over the radial area $r = 0\text{-}4^{o}$. The satellite analysis indicated no difference in the 1x1 area ($r \sim 1.4^{o}$), but a 25% greater amount of 3x3 area ($r \sim 4.2^{o}$)

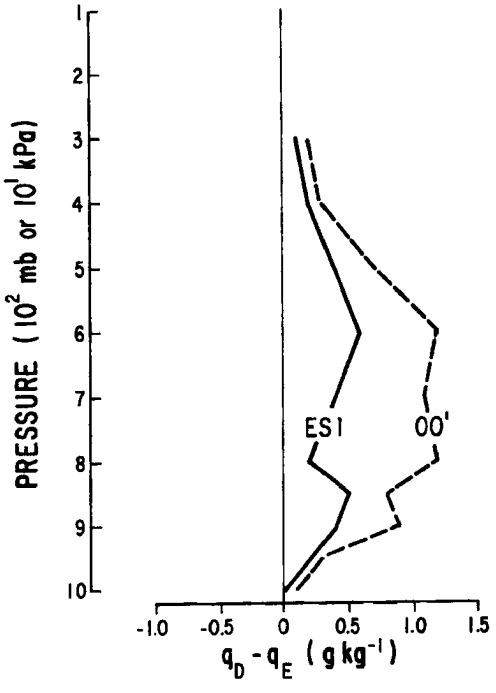

Fig. 9. Disturbance (r = 0-3°) minus environment (r = 3-7°) vertical moisture (q) profiles for the average developing (ES1) and non-developing (00') disturbances.

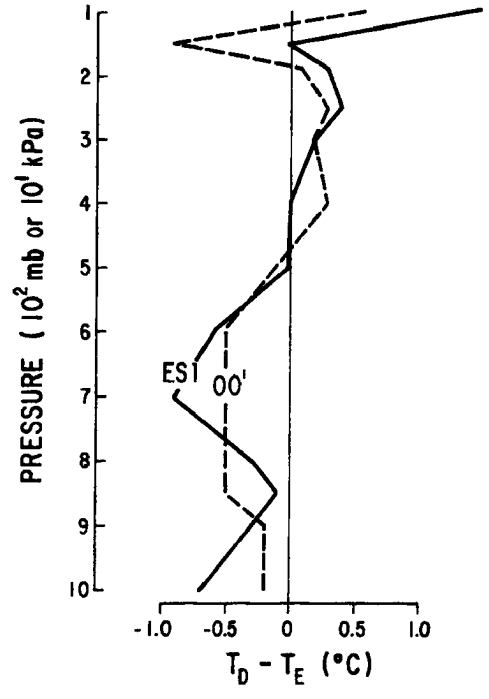

Fig. 10. Disturbance (r = 0-3°) minus environment (r = 3-7°) vertical temperature (T) profiles for the average developing (ES1) and non-developing (00') disturbances.

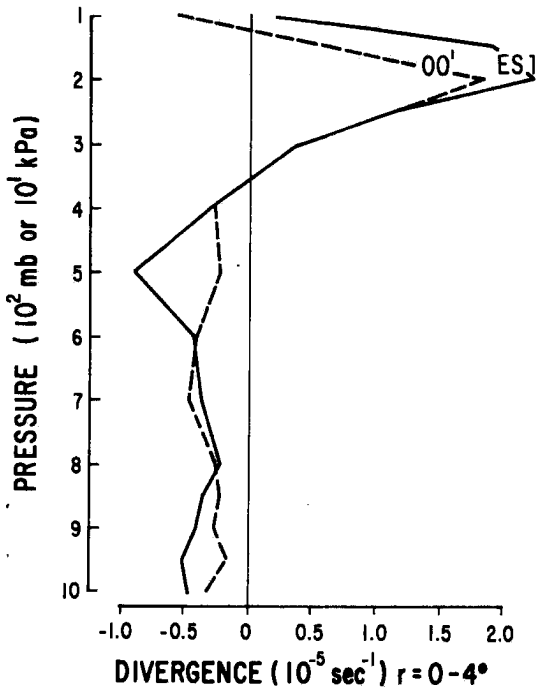

Fig. 11. Mean divergence within area r = 0-4° for the developing (ES1) and non-developing (00') disturbances.

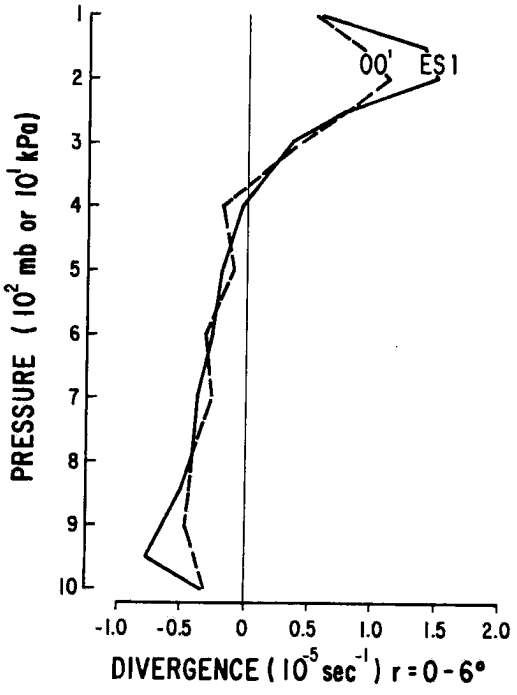

Fig. 12. Same as Fig. 11, except r = 0-6°.

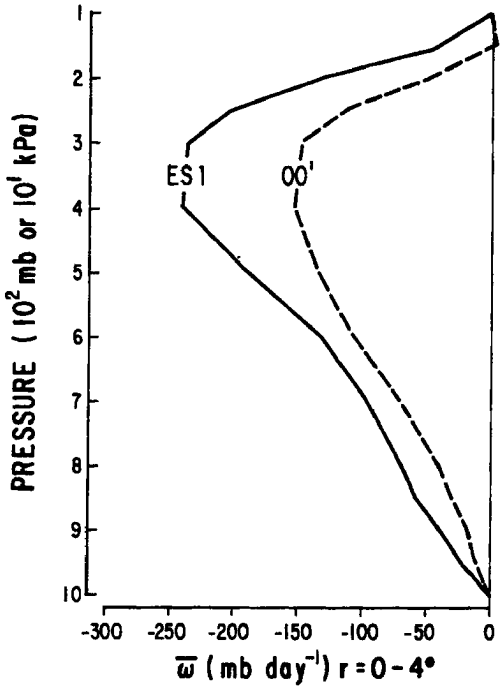

Fig. 13. Mean vertical motion within area r = 0-4° for the developing (ES1) and non-developing (00') disturbances.

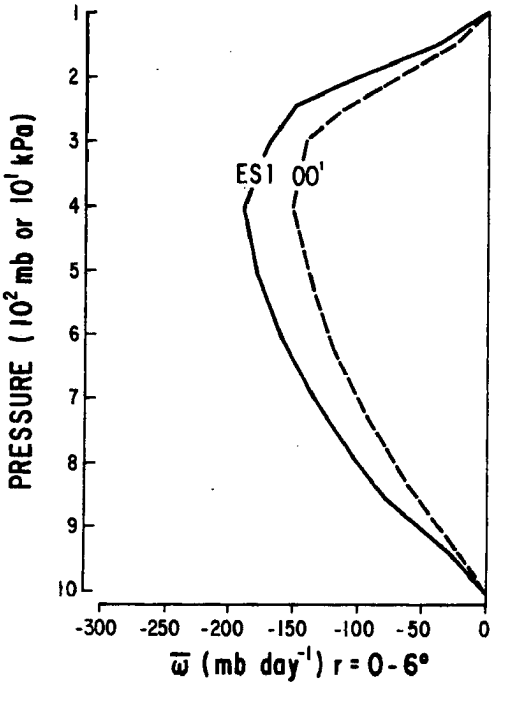

Fig. 14. Same as Fig. 13, except r = 0-6°.

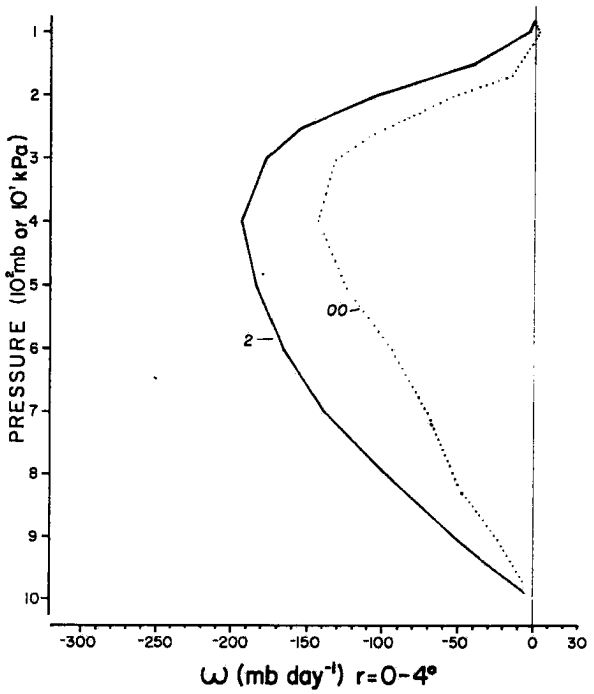

Fig. 15. Mean vertical motion within area r = 0-4° from Zehr's (1976) developing (Stage 2) and non-developing (Stage 00) disturbances.

deep convection in the developing systems as compared with the non-developing ones. Thus, the observed differences in mean vertical motion appear to be a result of outer radius convection differences.

4.3 Relative vorticity

The vertical profiles of relative vorticity computed from the tangential wind (V_T) for various radial areas are shown in Figs. 16 through 19. The Zehr (1976) vorticity profiles for the average developing and non-developing disturbances over the radial area r = 0-4° are also shown in Fig. 20 for comparison. Large differences ($\sim$ 2 to 1) exist between disturbance classes at nearly all levels. This is particularly striking at inner core radius ($r \leq 2^{\circ}$). Although the amount of deep convection is much the same in the central core between disturbance

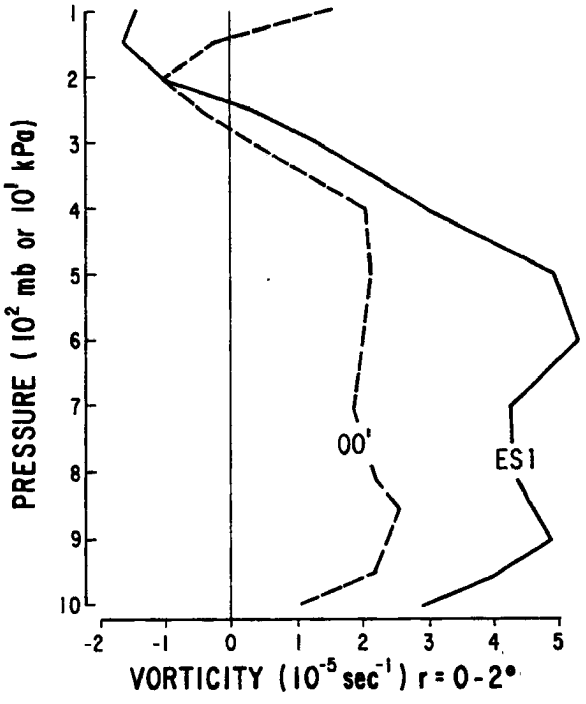

Fig. 16. Mean relative vorticity within area r = 0-2° for the developing (ES1) and non-developing (00') disturbances.

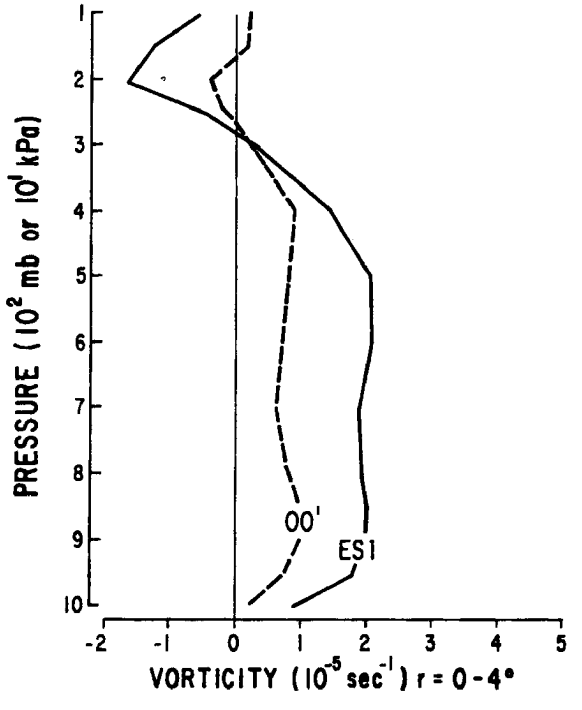

Fig. 17. Same as Fig. 16, except r = 0-4°.

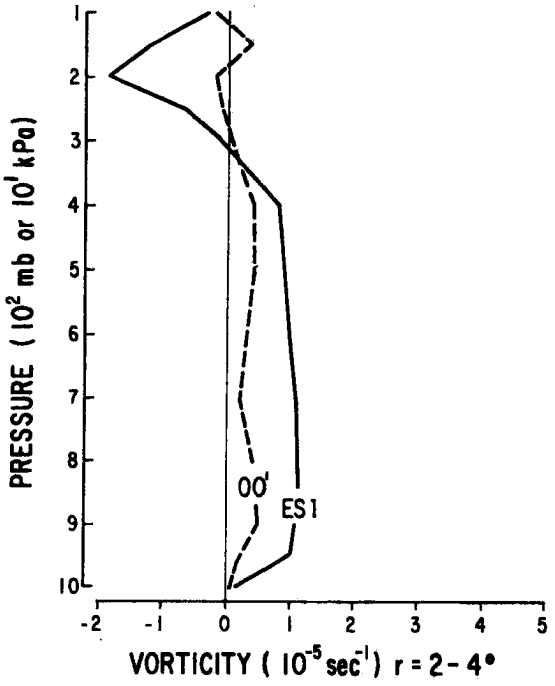

Fig. 18. Same as Fig. 16, except r = 2-4°.

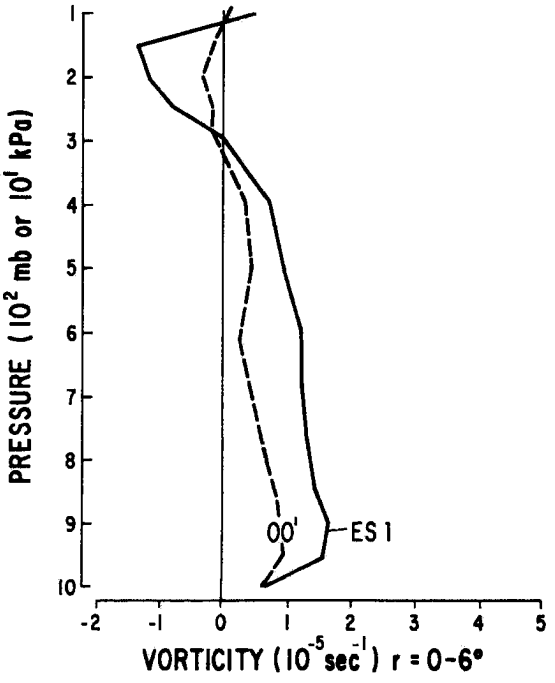

Fig. 19. Same as Fig. 16, except r = 0-6°.

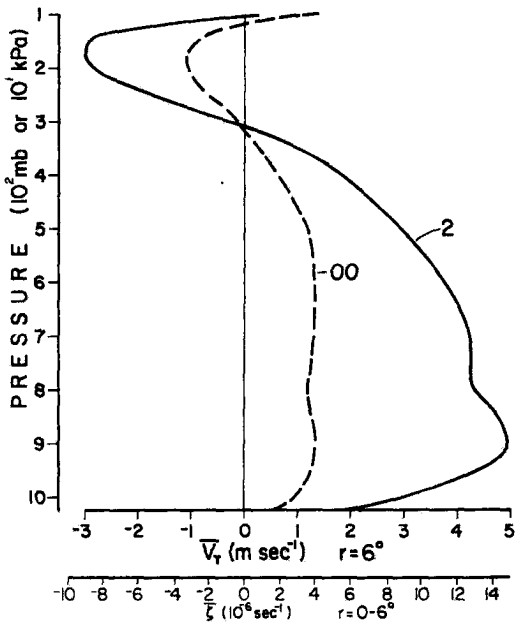

Fig. 20. Mean relative vorticity within area r = 0-6° (equivalent to mean tangential winds in r = 5-7° band) from Zehr's (1976) developing (Stage 2) and non-developing (Stage 00) disturbances.

classes there is significantly more vorticity in the developing systems. Upper-level (200 mb) relative vorticity (negative tangential wind) is observed to be much greater in the developing disturbances. This is a reflection of upper-level anticyclonic circulation differences between disturbance classes. The data of Zehr (1976) also shows a significant upper-level vorticity difference between disturbance classes at 200 mb (see Fig. 20).

Table 10 shows the mean relative vorticity ($\overline{\zeta}_r$) difference between 900 mb and 200 mb ($\overline{\zeta}_{r_{900mb}} - \overline{\zeta}_{r_{200mb}}$) for the developing and non-developing disturbances for various radial areas. When the upper and

TABLE 10

Mean Relative Vorticity ($\bar{\zeta}_r$) Differences Between 900 mb and 200 mb for the Developing (ES1) and Non-developing (00') Disturbances

	$(\bar{\zeta}_{r_{900\ mb}}$ minus $\bar{\zeta}_{r_{200\ mb}})(10^{-5}s^{-1})$	
Radial Area	Developing (ES1)	Non-developing (00')
$0-2^{o}$	5.9	3.4
$0-4^{o}$	3.6	1.3
$2-4^{o}$	2.8	.6
$0-6^{o}$	3.0	1.0
$4-6^{o}$	2.5	.8

lower-level vorticity values are combined, large differences ($\sim$ 4.5 to 1 at r = $2-4^{o}$) are observed to exist between disturbance classes. If the upper and lower tropospheric winds can be measured from the movement of clouds observed by geostationary satellites, these vorticity differences may provide a valuable operational parameter in forecasting disturbance intensification.

4.4 Upper and lower-level wind patterns

The streamline and isotach patterns at 950 and 200 mbs are shown in Figs. 21 and 22. Low-level winds (950 mb) indicate substantially more north-south shear in the average developing disturbance. Wind velocities at 200 mb are observed to be much the same. However, flow patterns are significantly different. These is much more anticyclonic flow in the developing cases, and more unidirectional flow in the non-developing disturbances.

Additional confirmation of the upper-level flow differences between disturbance classes is provided by an analysis of upper-level (cirrus)

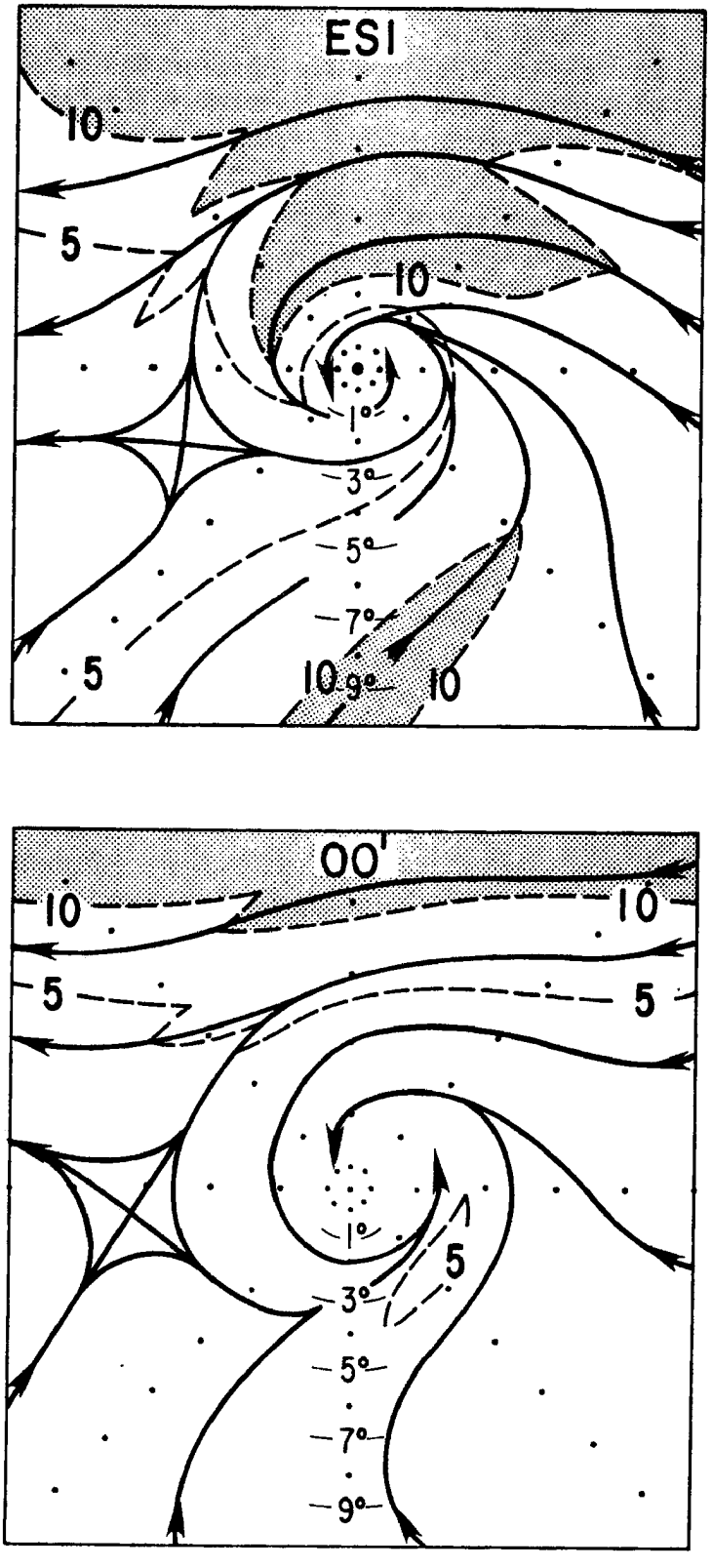

Fig. 21. Average isotach (m s^{-1}) and streamline analysis for the developing (ES1 - above) and non-developing (00' - below) disturbances at 950 mb.

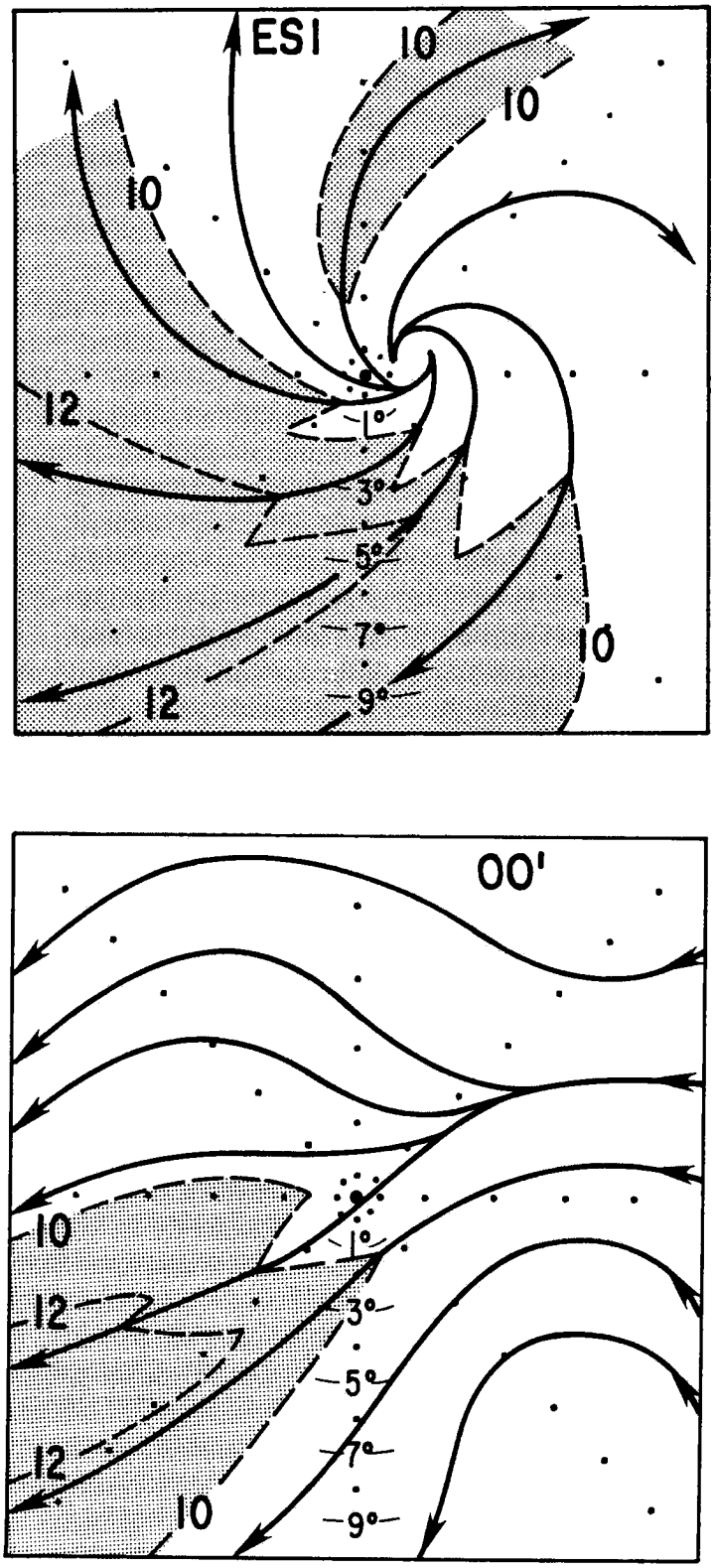

Fig. 22. Average isotach (m s^{-1}) and streamline analysis for the developing (ES1 - above) and non-developing (00' - below) disturbances at 200 mb.

winds in the visual satellite data and the 200 mb winds from the Zehr (1976) developing (Stage 2) and non-developing (Stage 00) rawinsonde composites. As indicated earlier, wind vectors corresponding to cirrus streaks resulting from deep convective cells were drawn on the visual satellite transparencies. Depending upon the characteristic flow pattern, the disturbance was qualitatively judged to either have an anticyclone aloft or not (see Table 3). Figure 23 shows a representative ($\sim$ 40%) sample of all satellite wind vectors. The most obvious difference is the flow to the north of the disturbances. The developing disturbance indicates anticyclonic flow, with a secondary outflow channel to the north. The feature which is most similar between composites is the strong northeasterly outflow in the southwest quadrant of the disturbances. A representative sample ($\sim$ 35%) of actual rawinsonde 200 mb winds of Zehr's (1976) developing (Stage 2) and non-developing (Stage 00) disturbance composites is shown in Fig. 24. Note the greater outflow to the north with the developing systems. The 200 mb v (meridional) component of the winds to the north by radial belts is shown in Fig. 25. These results support the satellite analysis. Large differences in poleward outflow are indicated. Gray (1968) has also indicated poleward outflow (200 mb) in developing disturbances at many oceanic locations where tropical cyclones form. Previous research (Sadler, 1967, 1976; Fett, 1966; Colón and Nightingale, 1963; and Riehl, 1975) has shown cyclone intensification to take place under favorable poleward upper tropopsheric flow features.

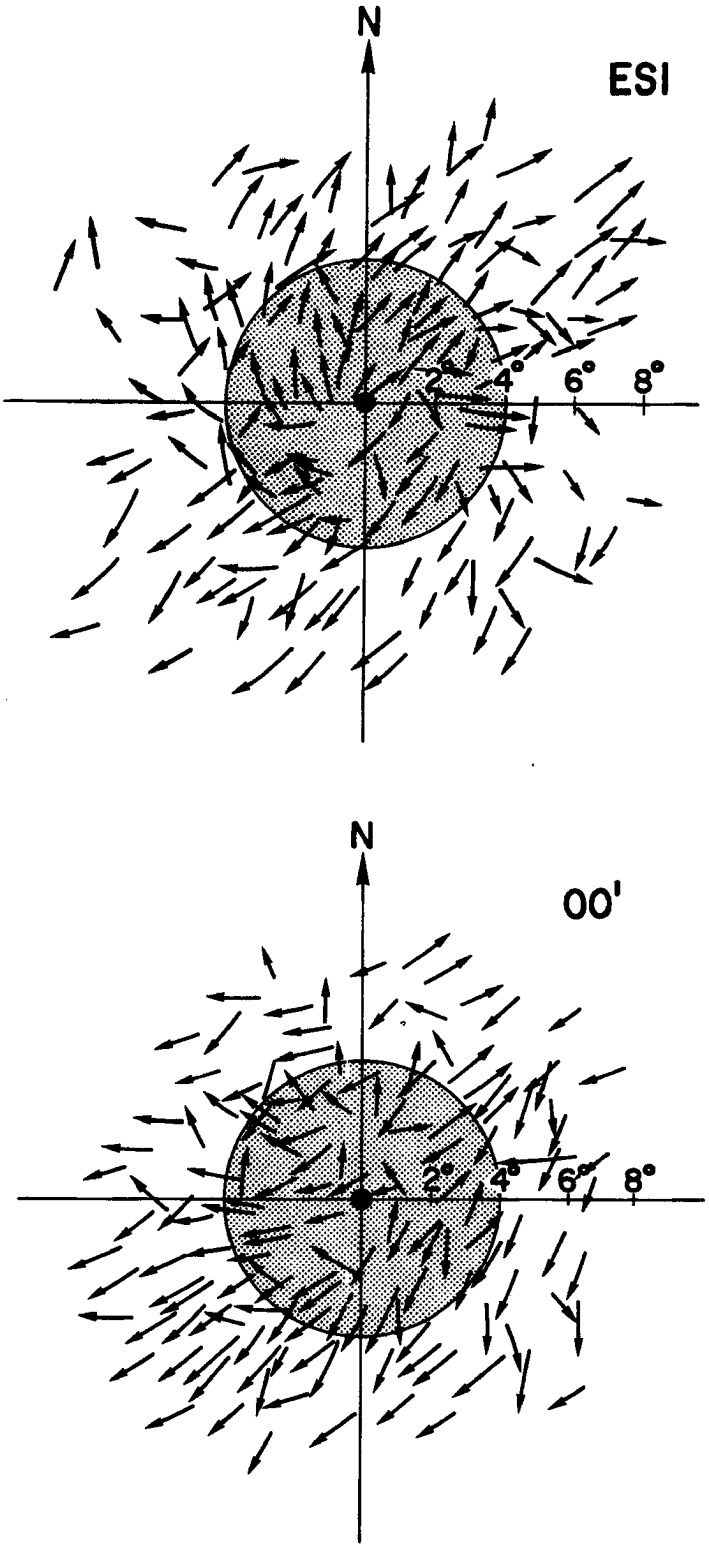

Fig. 23. A representative sample (∿ 40%) of cirrus level (∿ 200 mb) wind vectors determined from DMSP visual data for the developing (ES1 - above) and non-developing (00' - below) disturbances. The shaded area ($r = 4^{o}$) is an approximation of the average size of developing and non-developing disturbances.

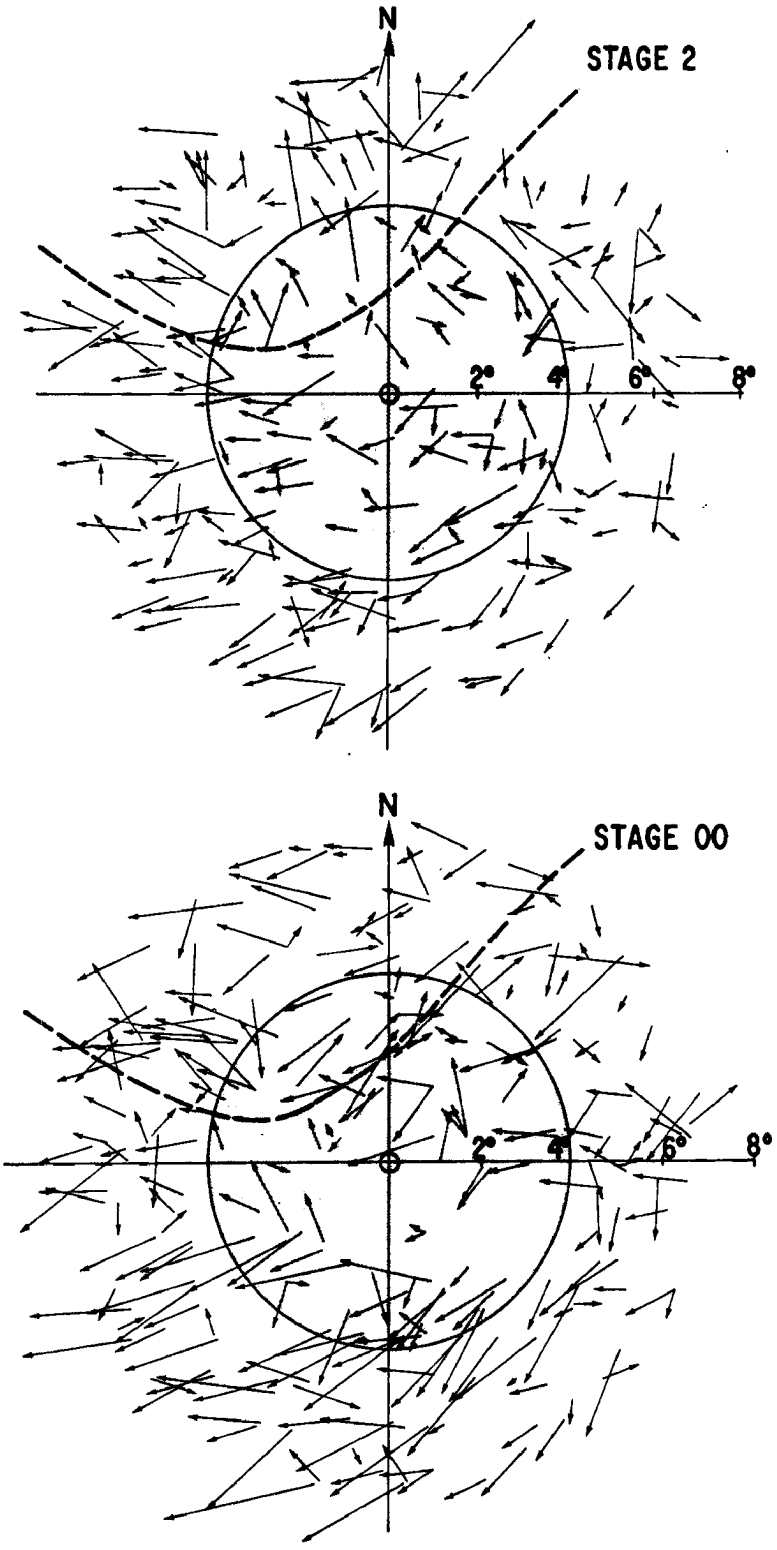

Fig. 24. A representative sample (∿ 35%) from Zehr's (1976) actual rawinsonde composited winds at 200 mb for his developing (Stage 2 - above) and non-developing (Stage 00 - below) disturbances. North of the dashed line shows largest differences between composites. The shaded area is the same as in Fig. 23.

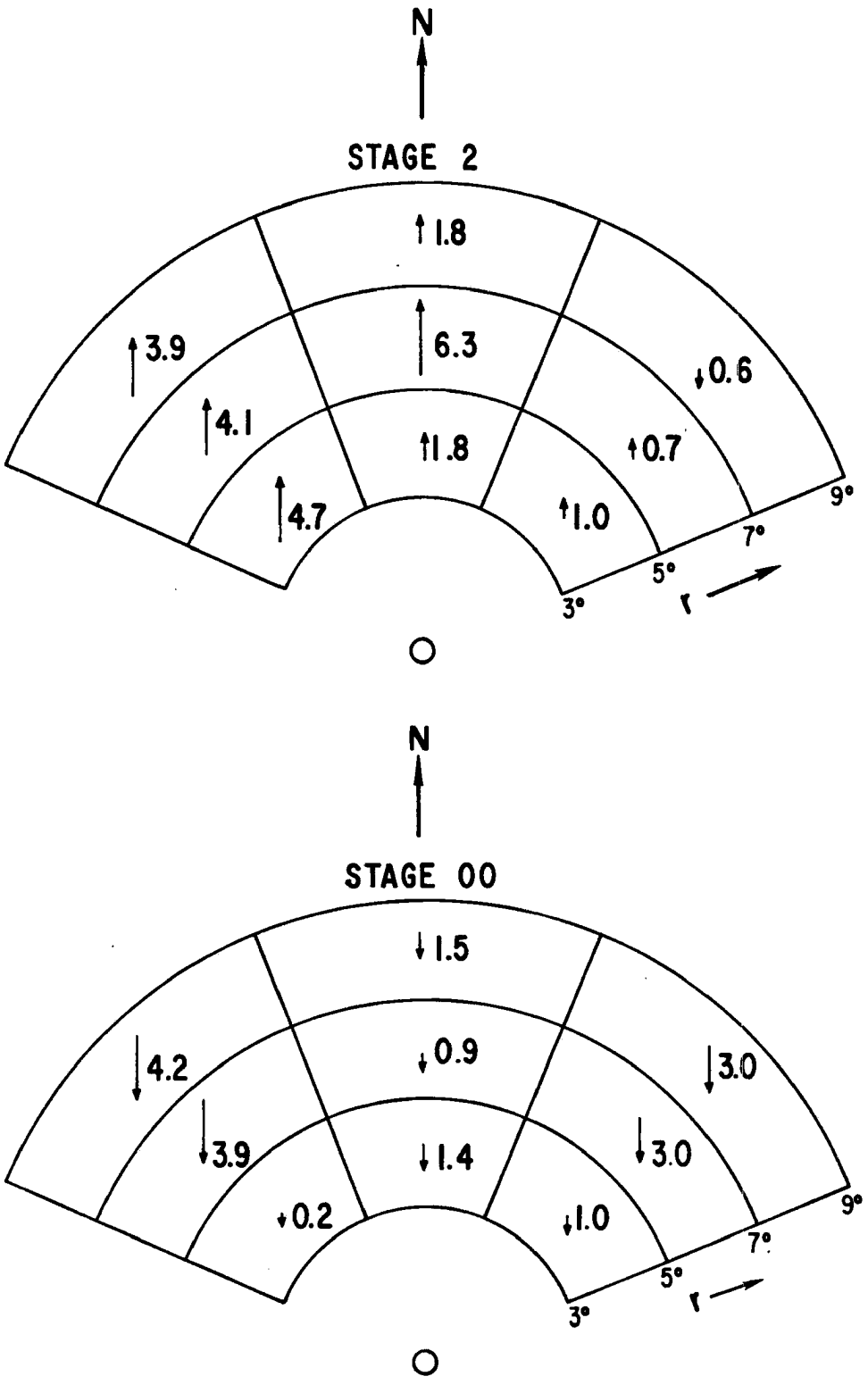

Fig. 25. Composited 200 mb meridional (v) component of the wind (m s^{-1}) from Zehr's (1976) developing (Stage 2) and non-developing (Stage 00) rawinsonde composites. Each octant-belt represents an average of about 30 rawinsonde reports.

4.5 Vertical shear

The vertical shears of the zonal wind ($r = 0\text{-}3^{o}$) for the average developing (ES1) and non-developing (00') disturbances are shown in Fig. 26. The vertical shear of the zonal wind between 850 mb and 200 mb ($u_{850\ mb} - u_{200\ mb}$) is 1.6 m s^{-1} and 5.8 m s^{-1} for the developing and non-developing disturbances, respectively. Gray (1968) has previously indicated that tropospheric vertical wind shears (meridional and zonal) are nearly zero for disturbance genesis in the Pacific, West Indies, and North Indian Oceans.

The u (zonal) component of the average speed of movement for disturbance classes is also displayed in Fig. 26. The average speed of movement of the developing disturbance closely approximates the zonal wind at all levels. A much larger difference is observed between the propagation speed of the non-developing disturbance and the zonal wind below 600 mb. The average developing disturbance is ventilated by flow blowing through from east to west above 600 mb, while the average non-developing disturbance is ventilated from west to east through the entire depth of the troposphere. Thus, the developing systems appear to lose substantially less moisture and heat energy through horizontal ventilation or blow-through. This has been extensively discussed in reports by Gray (1968, 1975) and Zehr (1976).

Summary. In general, the rawinsonde results of this study are in good agreement with previous rawinsonde compositing studies of Williams and Gray (1973) and Zehr (1976) which were based on larger data samples. This lends confidence to the results of this study.

Rawinsonde analysis indicates that the magnitude of tropospheric convergence-divergence and mean vertical motion through the disturbances

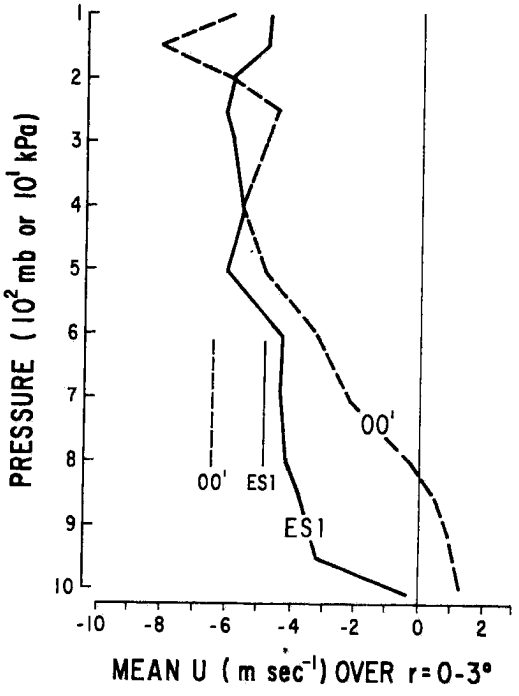

Fig. 26. Average zonal wind (u) within area r = 0-3° for the developing (ES1) and non-developing (00') disturbances. The u-component of the average propagation speed of the developing and non-developing disturbance is also indicated by the vertical solid and dashed lines.

were not well correlated with their intensification potential. The previous chapter satellite cloudiness information provides additional support for this contention. Temperature and moisture differences also do not appear to be significantly different. Large differences between disturbance classes, which are likely significant genesis parameters are:

1) lower tropospheric relative vorticity,

2) cirrus level (∿ 200 mb) outflow patterns to the poleward side of the disturbance, and

3) vertical shear and wind blow-through.

5. CLOUDINESS VARIABILITY OF INDIVIDUAL DEVELOPING AND NON-DEVELOPING DISTURBANCES

The complex movement and variability of cloud clusters and disturbance convective cores within Atlantic disturbances has been documented by Martin and Suomi (1972) and many other satellite meteorologists. Large daily variability of penetrative convection and overall cloudiness was also observed in this investigation.

5.1 Representative sample comparisons

As indicated earlier, the 3x3 grid area ($r \sim 4.2^{o}$) is most representative of the disturbance. The daily variability of cloudiness in this area will now be discussed. A randomly ordered sample representing approximately 40% of the total satellite picture set was assumed sufficiently large to determine this daily variability. Variability (V) is best shown by percent deviation from the mean or average state and is defined as:

$$V = \left(\frac{x - \bar{x}}{\bar{x}} \right) X \quad 100$$

where x = individual sample value

$\bar{x}$ = composited or average value.

Variability determinations for the traced penetrative convection (data set 2) and total cirrus (data set 3) are presented in Figs. 27 and 28. A few other time periods exhibited even larger variability but these were not plotted. The dashed lines represent the mean of plotted cloudiness samples above and below 0 percent deviation.

As expected, the developing disturbance exhibits the same degree of variability in deep convection and total cirrus as the non-developing

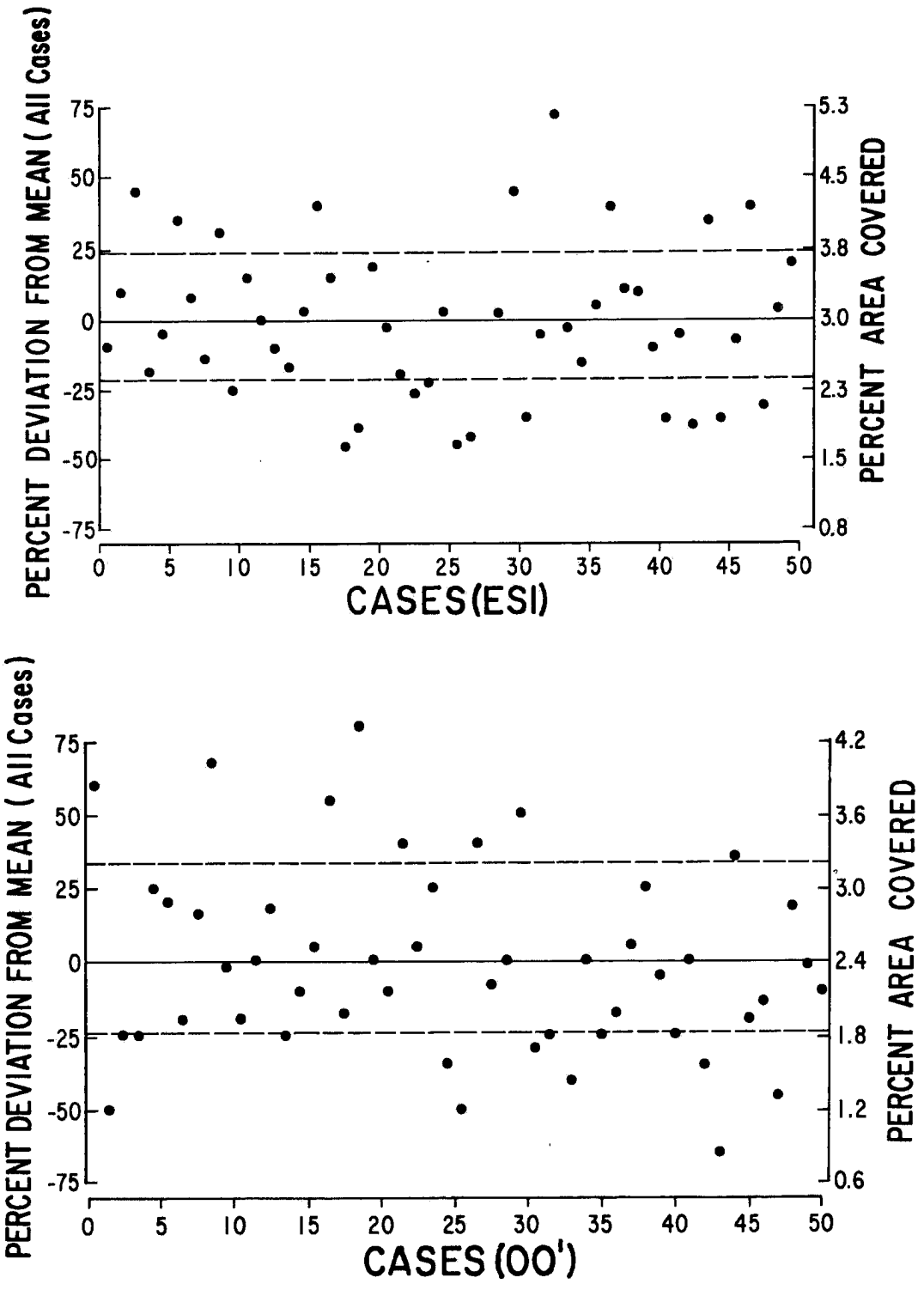

Fig. 27. A representative sample ($\sim$ 40%) of the daily variability displayed by penetrative convection within the 3x3 area ($r \sim 4.2^{o}$) for the developing (ES1) and the non-developing (00') disturbances. The dashed lines represent the mean of plotted convection samples above and below the case mean values.

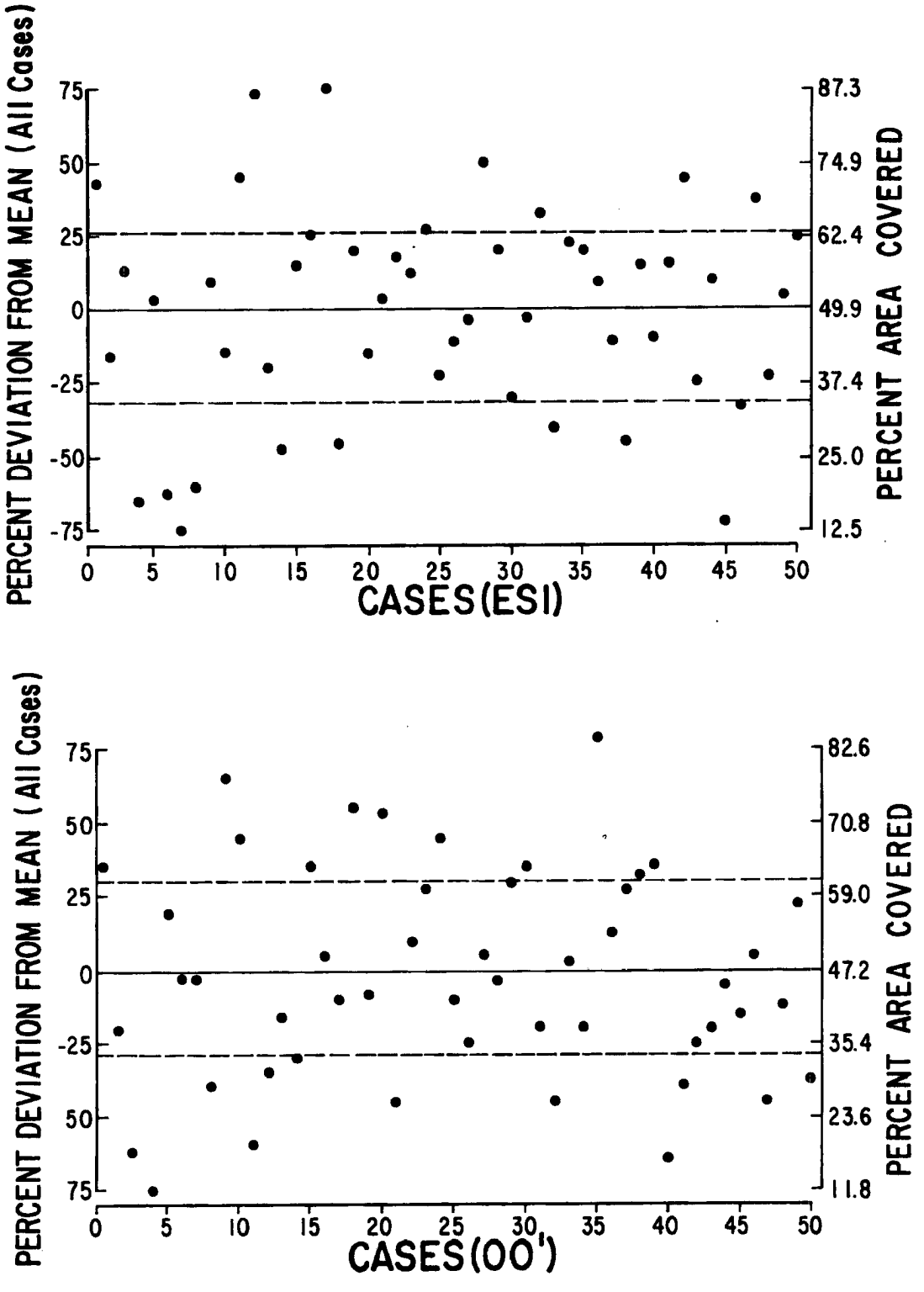

Fig. 28. A representative sample (∿ 40%) of the daily variability displayed by total cirrus within the 3x3 area (r ∿ 4.2°) for the developing (ES1) and non-developing (00') disturbances. The dashed lines represent the mean of plotted cirrus samples above and below the case mean values.

disturbance. The amount of deep convection in the developing disturbance is conservative only in the sense that it does not become significantly greater as the system intensifies. The percent area covered by deep convection over the 3x3 grid ($r \sim 4.2^{o}$) increased by an average of only 5% from the first to the last picture for the 53 developing (ES1) cases. Hence, the developing disturbances display a large daily variability in the amount of convection and the chance of increasing or decreasing this amount from the initial disturbance to some time later is about the same. The same conclusion is resulting from the study of Arnold (1977). He shows cyclone strength to be nearly independent of convection amount in four different groups of tropical cyclones stratified by intensity. The physical processes responsible for the large daily variations in convection and cirrus are not known.

As the average time between two consecutive morning and early afternoon pictures of the same disturbance is only 4 hours (i.e., 08 LT to 12 LT), diurnal variability of deep convection (Jacobson and Gray, 1976) cannot be used as an explanation for the large cloudiness changes observed in Figs. 27 and 28. The average cloudiness of the 12 LT picture was only slightly greater than the 08 LT pictures.

5.2 Individual case variability

Two typical cases from the developing and non-developing samples are presented for illustration. Individual case satellite pictures are shown in Figs. 29, 31, 33 and 35. The corresponding variability computations for total cirrus and penetrative convection within the 3x3 area are presented in Figs. 30, 32, 34 and 36. The large daily variability is clearly evident. The amount of penetrative convection

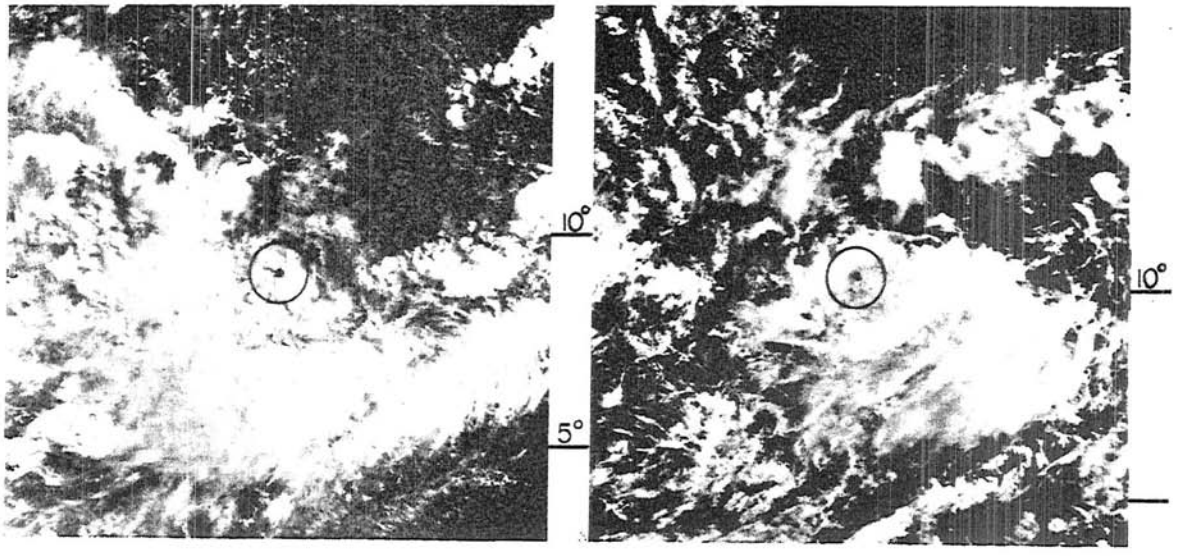

3/0912 LT 4/1358 LT

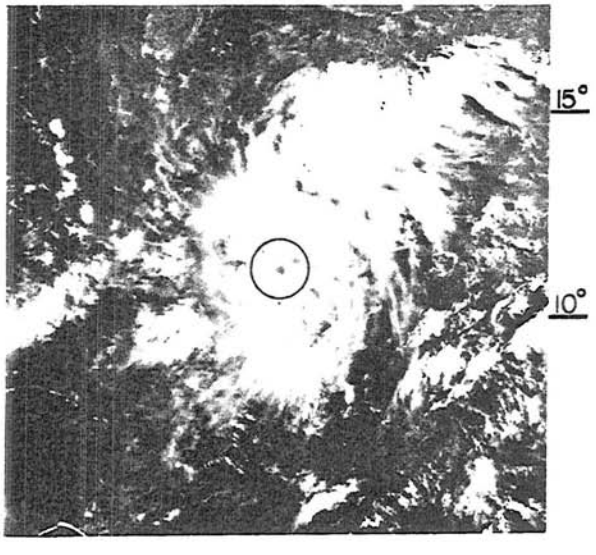

5/0958 LT

Fig. 29. DMSP pictures of an individual developing disturbance case (1) history during the time interval 3-6 July, 1972.

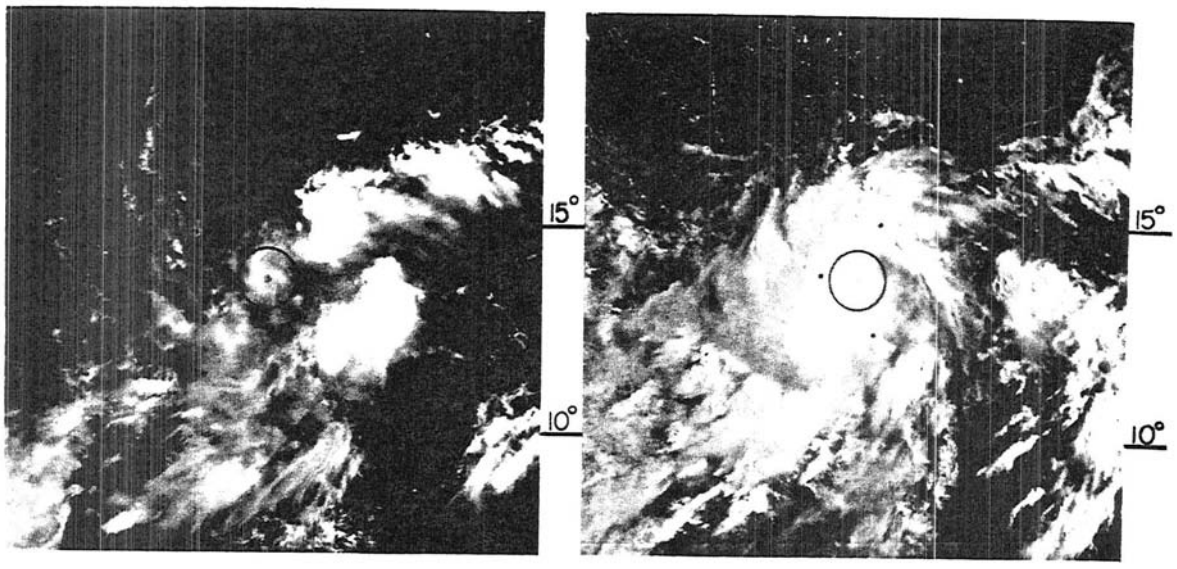

5/1342 LT 6/0931 LT

Fig. 29. Continued.

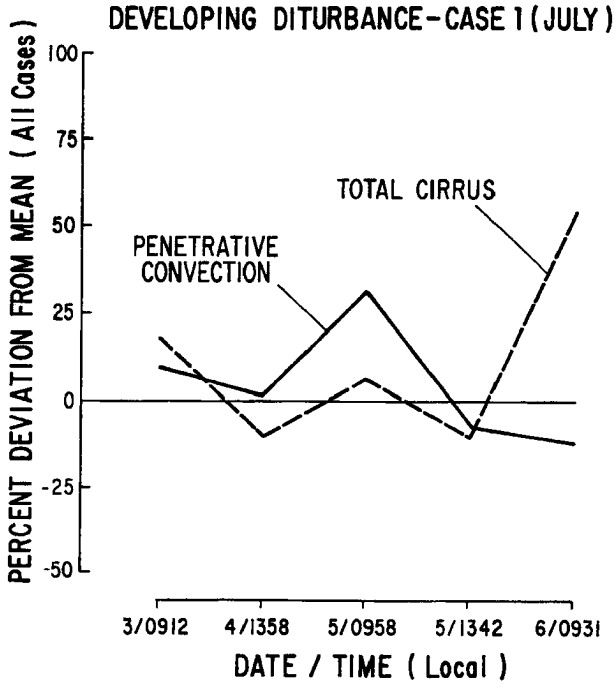

Fig. 30. Daily variability of penetrative convection and total cirrus within the 3x3 area ($r \sim 4.2^{o}$) of developing disturbance case (1) corresponding to Fig. 29.

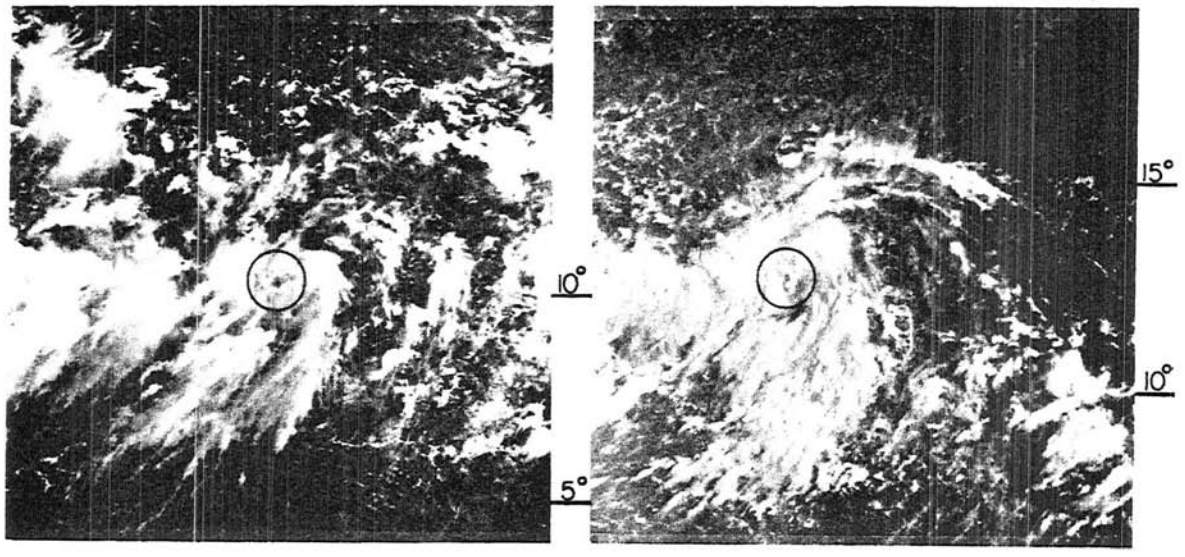

8/1318 LT

9/0830 LT

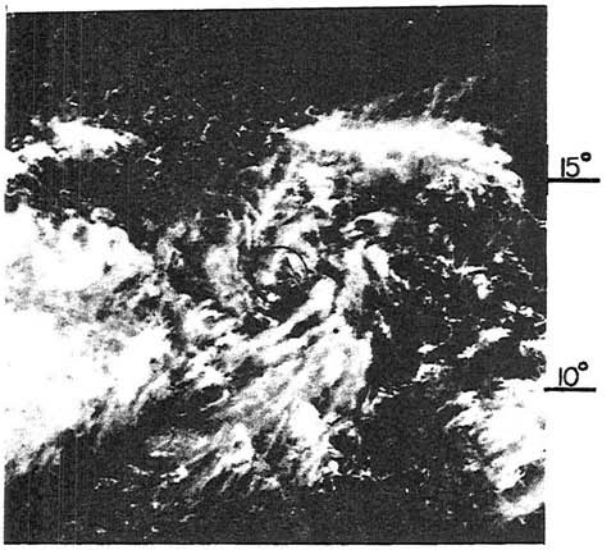

9/1303 LT

Fig. 31. DMSP pictures of an individual developing disturbance case (2) history during the time interval 8-11 September, 1972.

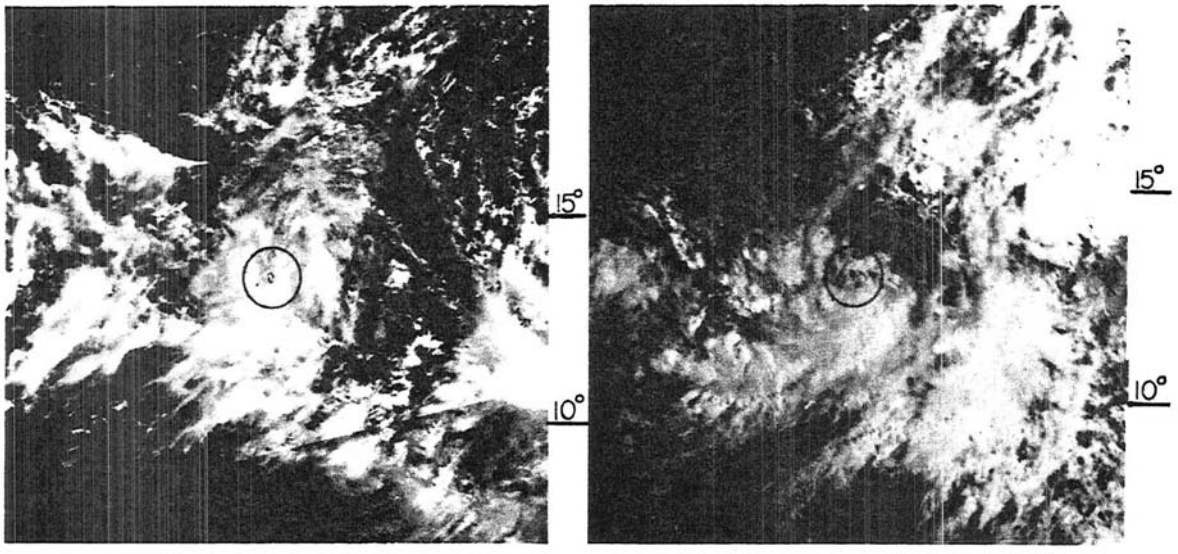

10/1249 LT 11/0916 LT

Fig. 31. Continued.

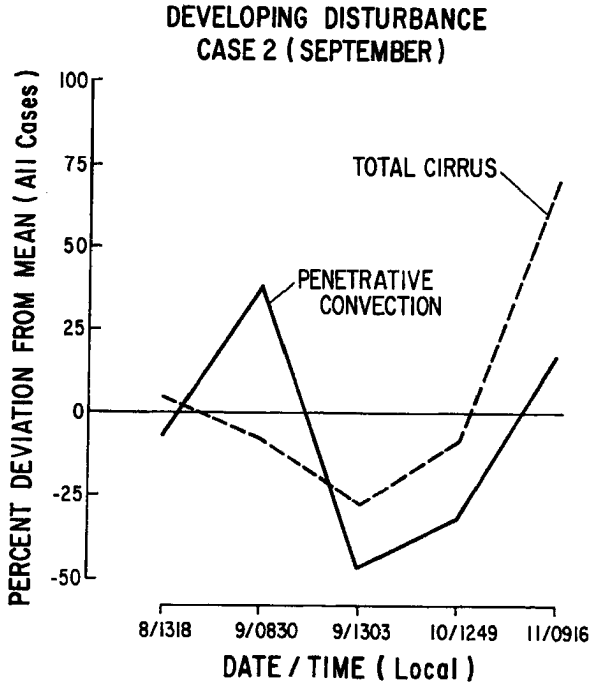

Fig. 32. Daily variability of penetrative convection and total cirrus within the 3x3 area ($r \sim 4.2^{o}$) of developing disturbance case (2) corresponding to Fig. 31.

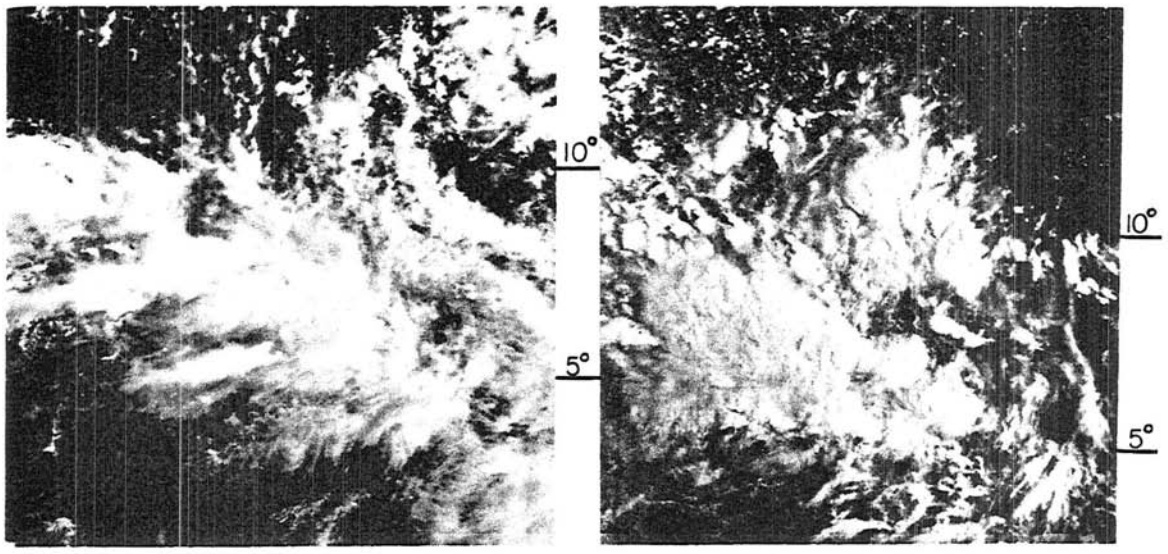

30/1313 LT

1/0826 LT

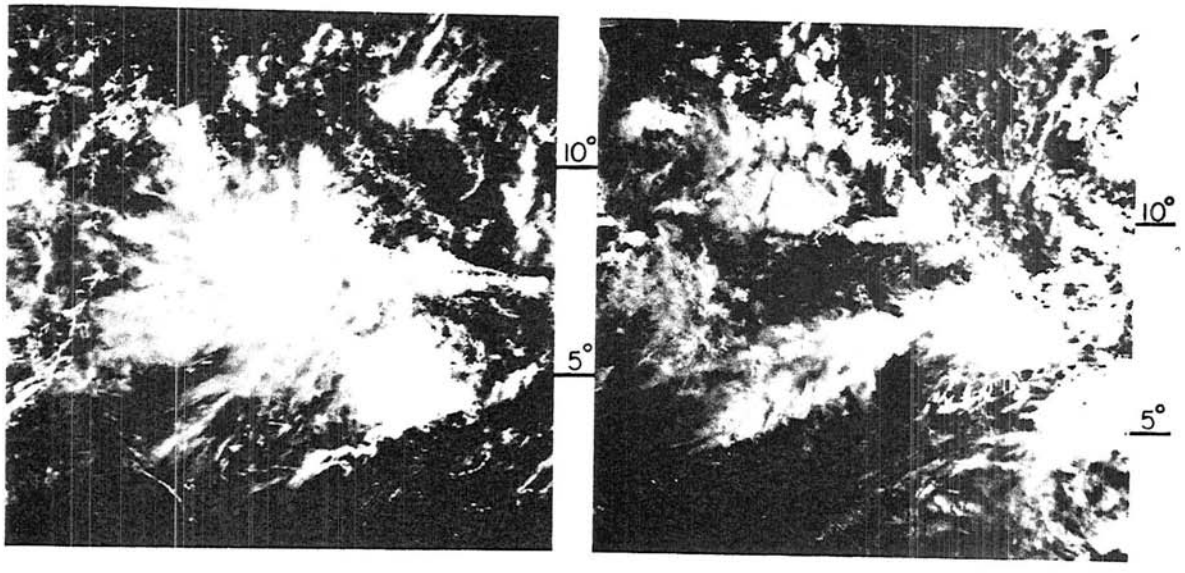

Fig. 33. DMSP pictures of an individual non-developing disturbance case (1) history during the time interval 30 June - 2 July, 1972.

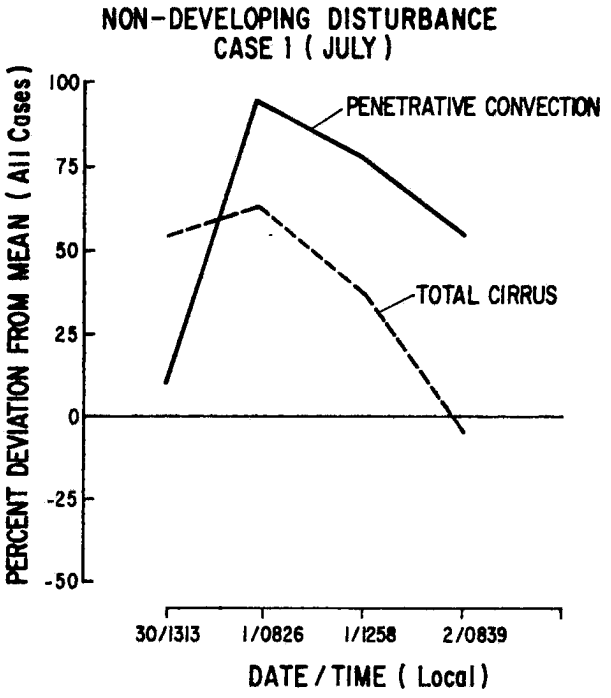

Fig. 34. Daily variability of penetrative convection and total cirrus within the 3x3 area ($r \sim 4.2^{o}$) of non-developing disturbance case (1) corresponding to Fig. 33.

is observed to be above the average of all cases in the two non-developing disturbance examples, yet no intensification takes place. Convection and cirrus amounts also show large variations in the developing cases which later intensify into typhoons. Upper-level flow is observed to become anticyclonic in the two developing cases, while remaining generally unidirectional in the non-developing disturbances. From an operational point of view, the type of cirrus level derived flow pattern appears to be a far better parameter to the forecasting of disturbance intensification than is satellite total cloud amount.

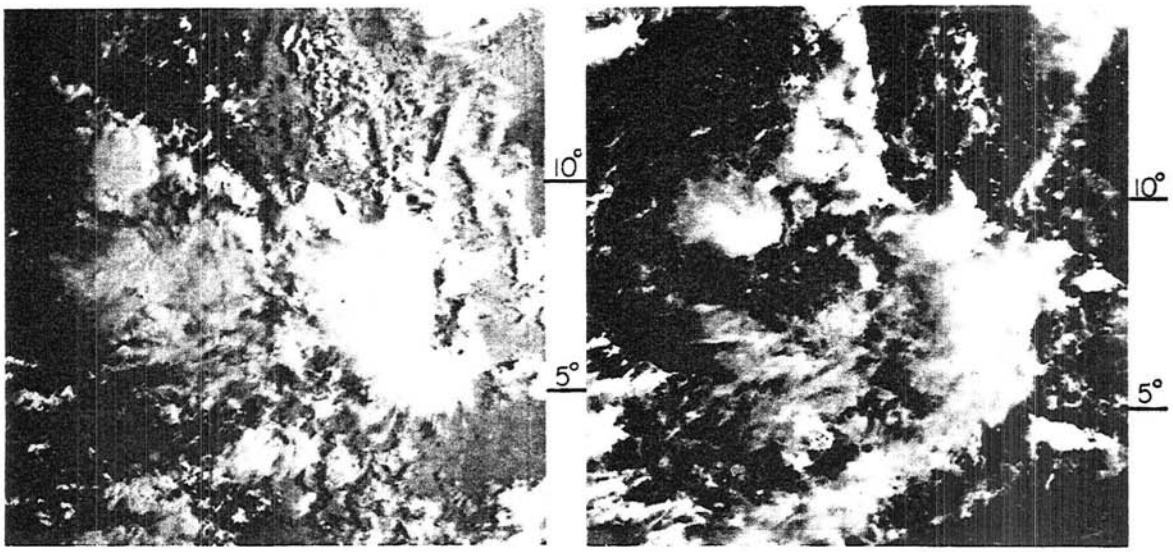

23/0930 LT

23/1346 LT

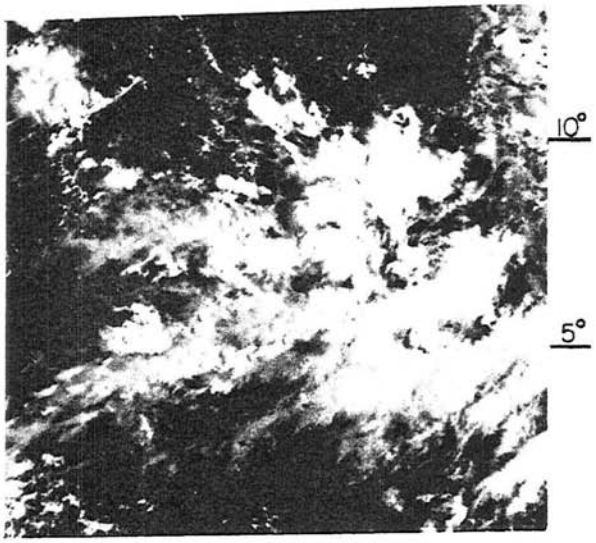

24/0904 LT

Fig. 35. DMSP pictures of an individual non-developing disturbance case (2) history during the time interval 23-25 August, 1972.

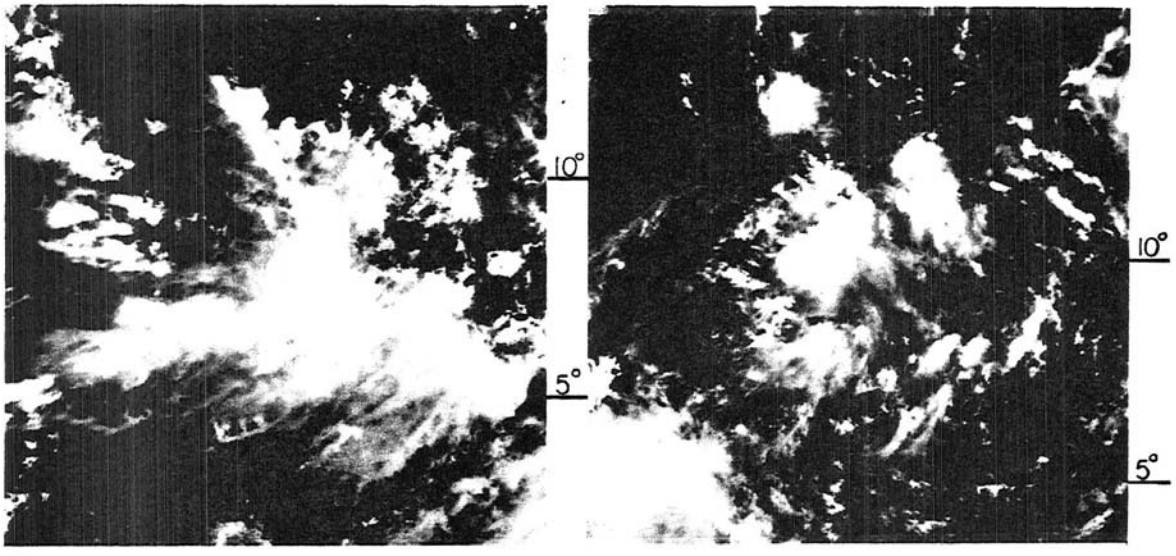

24/1321 LT 25/1317 LT

Fig. 35. Continued.

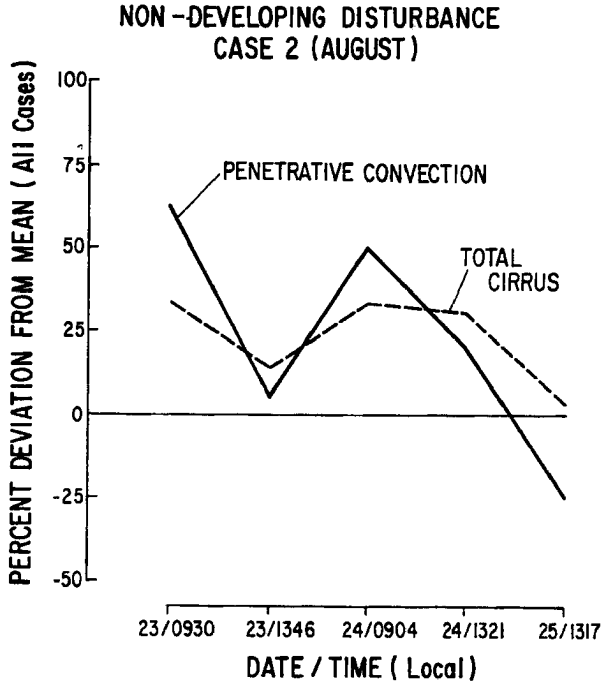

Fig. 36. Daily variability of penetrative convection and total cirrus within the 3x3 area ($r \sim 4.2^{\circ}$) of non-developing disturbance case (2) corresponding to Fig. 35.

6. THE CYCLONE VORTEX

The most obvious feature in the satellite data of both disturbance classes is the multiple and separate cloud cluster groups within the individual disturbance systems (see Figs. 3 and 4). These elements could not be well distinguished by the previous daily ESSA (NOAA) satellite which tended to merge cloud groups. The high resolution DMSP data reveals areas of suppressed convection or even clear regions within the disturbances. This feature is most apparent in the IR data which is not affected by sun angles and the difficulty in distinguishing albedos of cirrus and deep convection.

6.1 Centers of circulation

Near the end of this study, the author closely inspected the visual and infrared transparencies of the developing disturbances and observed that distinct areas of minimum convection coincided with the forming cyclone centers. This feature is apparent in Figs. 4 and 37. Additional documentation is provided by Arnold (1977). These pictures reveal that the majority of the circulation centers of low latitude (i.e., ITCZ) disturbances form somewhere within the disturbance cloud system. Arnold (1977), using high resolution DMSP data in coordination with the Joint Typhoon Warning Center, was the first to observe this phenomena with the DMSP data from Guam and infer that this is likely a characteristic feature in the early cyclone genesis process. As early as 1971, Arnold (1977) hypothesized that the area of suppressed convection near the circulation center was probably indicative of some type of mass subsidence. Documentation and a discussion of his early findings are described in more detail in his 1977 paper.

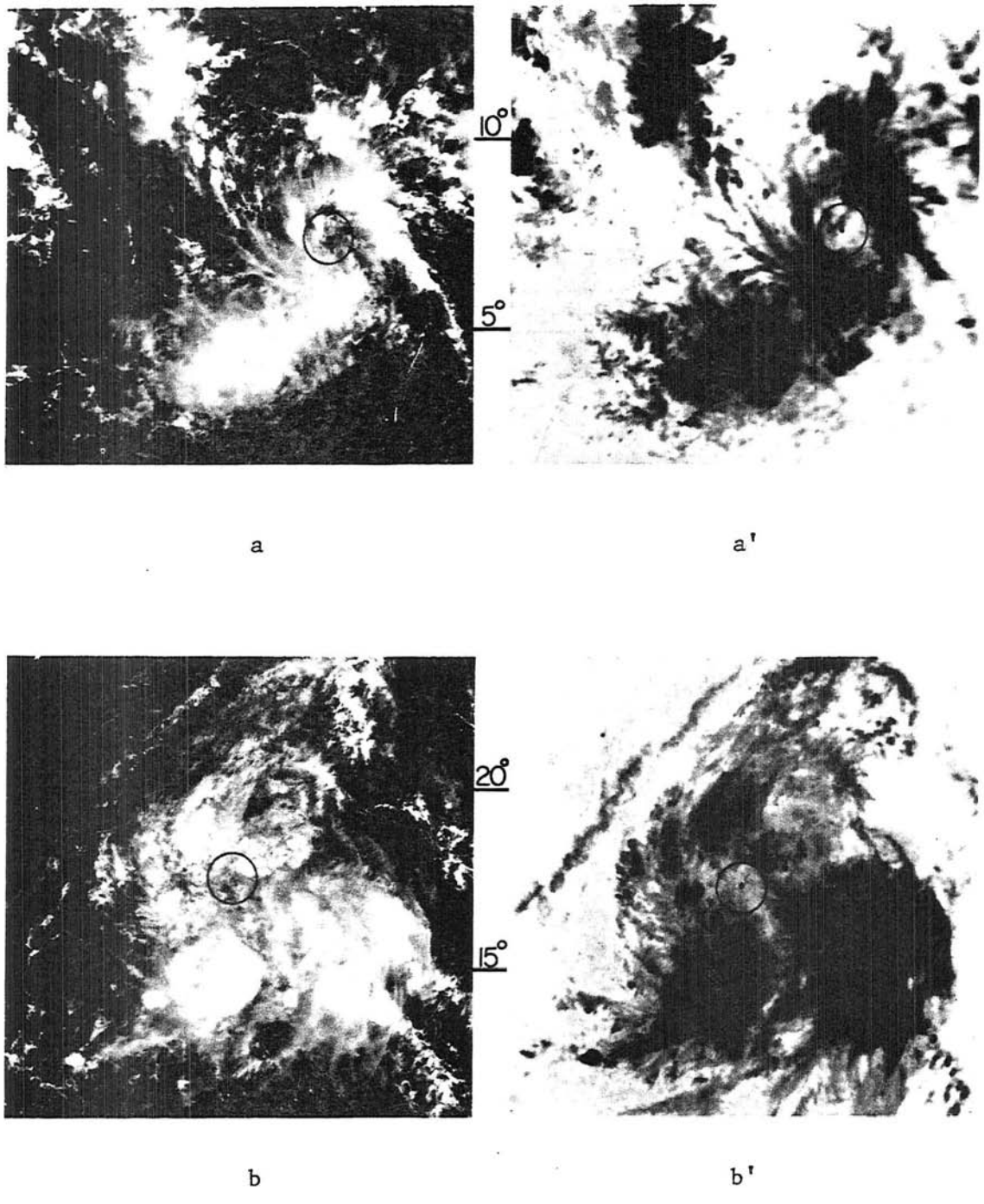

Fig. 37. Six DMSP cases visual (a-f) and the corresponding IR (a'-f') of early stage (maximum wind < 10-12 m s^{-1}) developing disturbances which demonstrate the area of suppressed convection within the disturbance's circulation center indicated by circle (r ∿ 83 km).

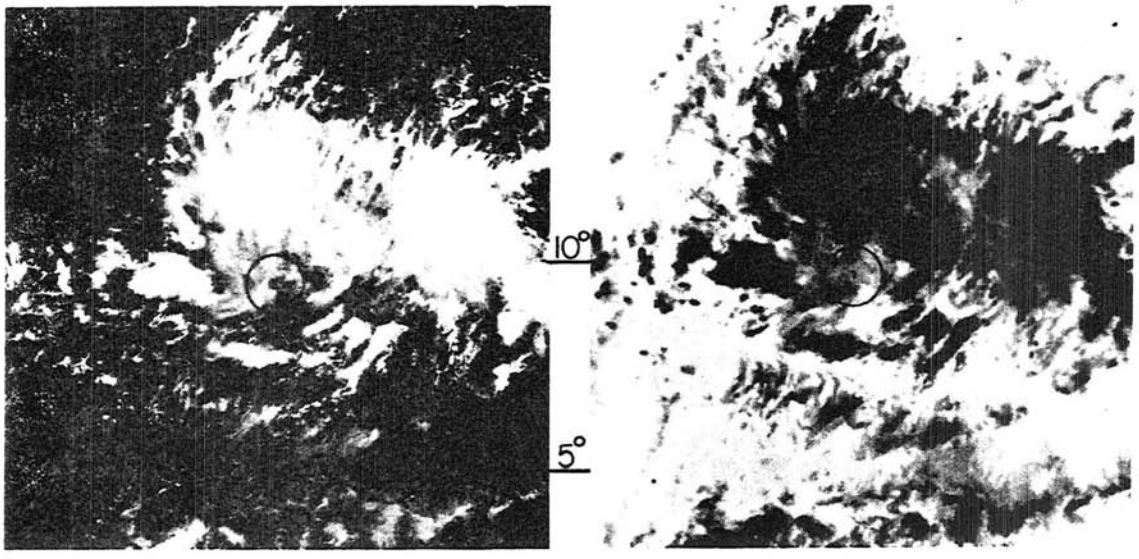

c c'

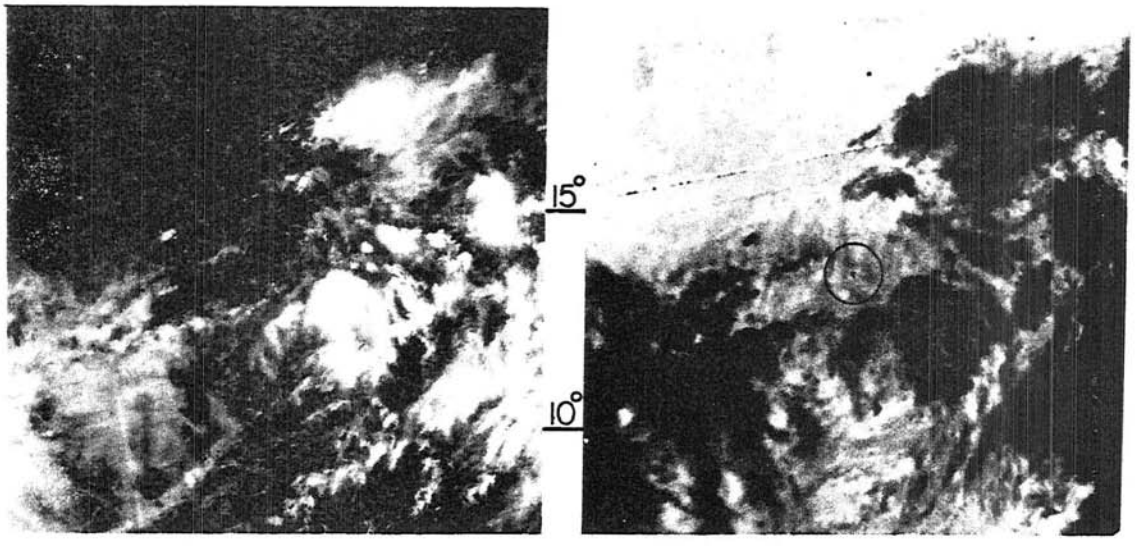

d d'

Fig. 37. Continued.

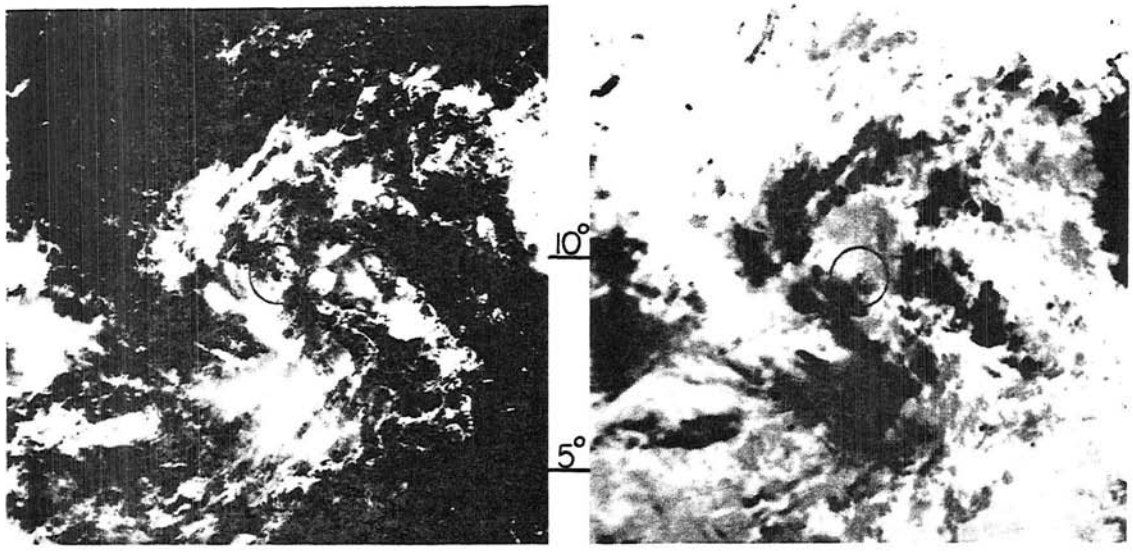

e e'

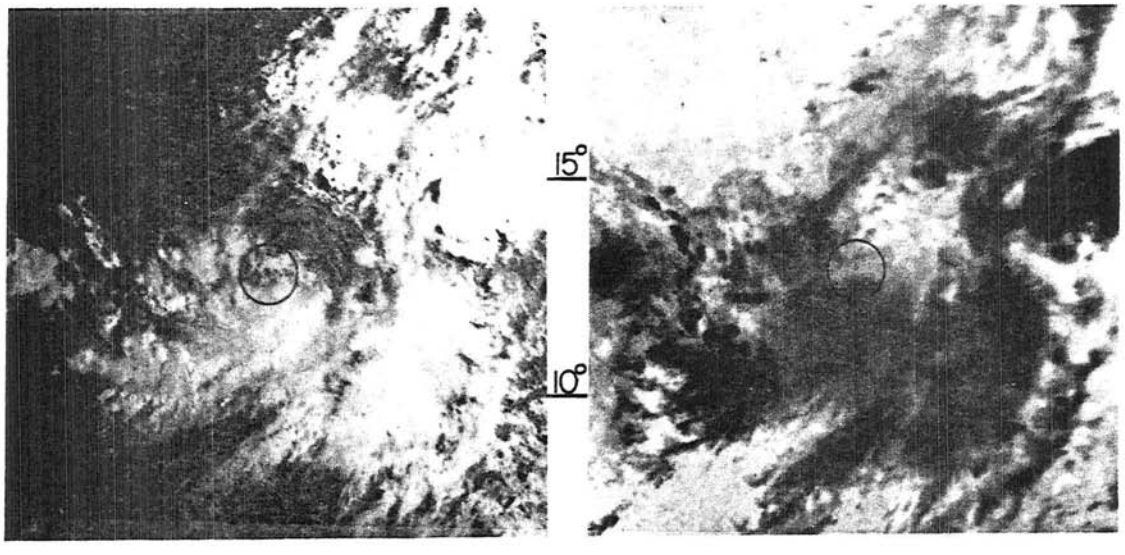

f f'

Fig. 37. Continued.

It is obvious that some type of local subsidence is also occurring in the non-developing disturbances (see Fig. 3). A re-inspection of the non-developing disturbances by the author revealed that at least 12% of the non-developing systems also possessed similar type circulation centers. These centers were similarly located in regions of suppressed convection (Fig. 38 gives 4 examples).

Centers of circulation have previously been observed to exist outside of or on the edge of the disturbance cloud clusters. Fritz (1962), Fett (1964), Merritt (1964), Fritz et al. (1966), Yanai (1968), Frank and Johnson (1969), Oliver and Anderson (1969), Lopez (1973), Thompson and Miller (1974), Sadler (1975), Smith et al. (1975) and Wright (1976) have all documented or discussed the existence of low-level circulation centers adjacent to disturbance cloud systems. The centers often appeared to act as the center for the developing cyclone. Clouds gradually develop around these centers. These disturbances were usually in the Atlantic or the Pacific trade wind equatorial trough.

6.2 Implications for cyclone genesis

The satellite cloud analysis showed the amount of deep convection and total cirrus to be much the same within the developing and non-developing disturbances. Implications are that the amount of direct sensible heat gain by condensation and net radiational differences induced by the cirrus canopies is also much the same and these latter features may not be fundamental parameters at distinguishing genesis.

Results of this and the concurrent Arnold (1977) study provide substantial documentation indicating the most efficient warming mechanism is localized areas of dynamically forced subsidence. If areas of

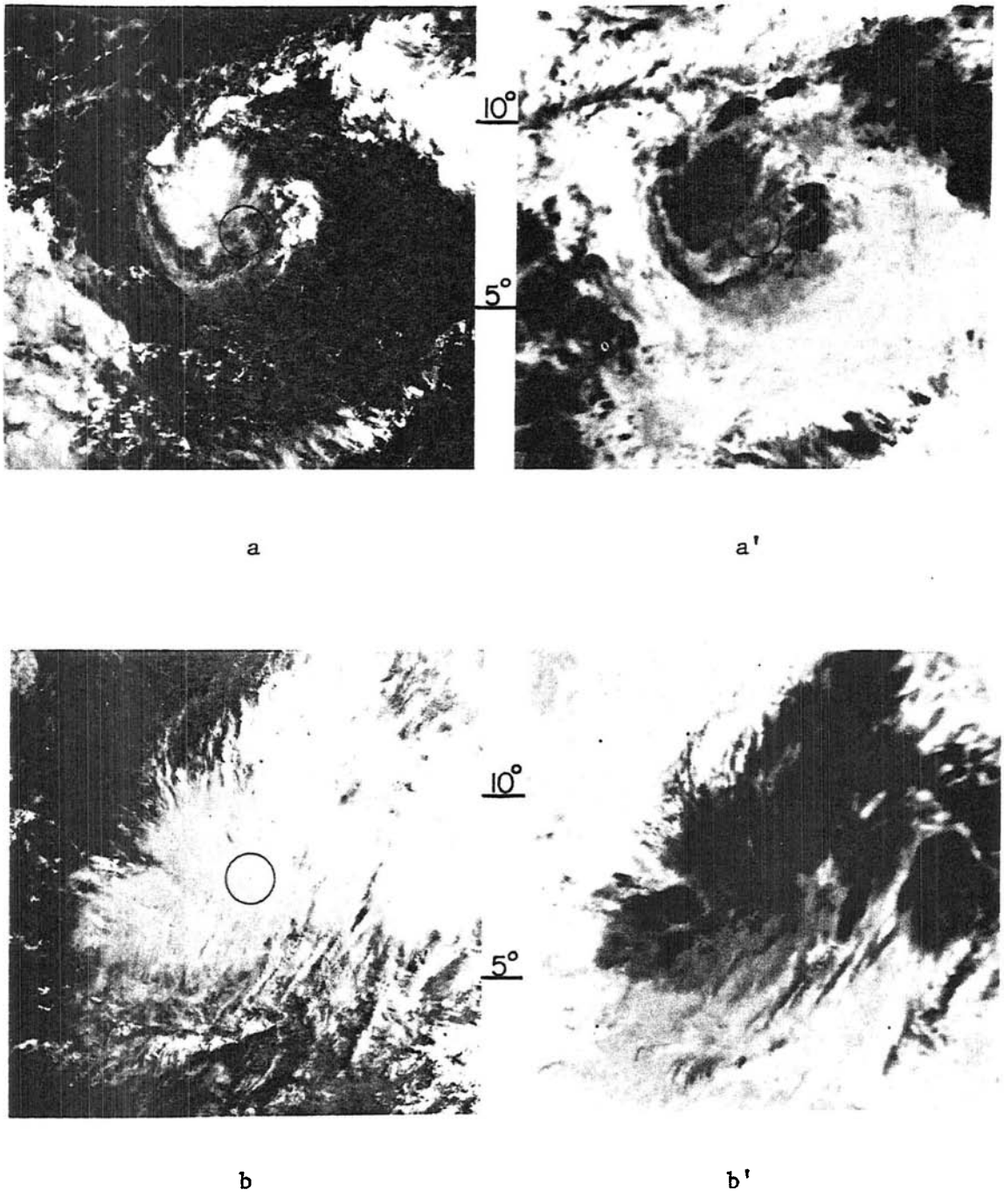

Fig. 38. Four DMSP cases visual (a-d) and the corresponding IR (a'-d') of non-developing disturbances which also demonstrate an area of suppressed convection within the disturbance's circulation center indicated by circle ($r \sim 83$ km).

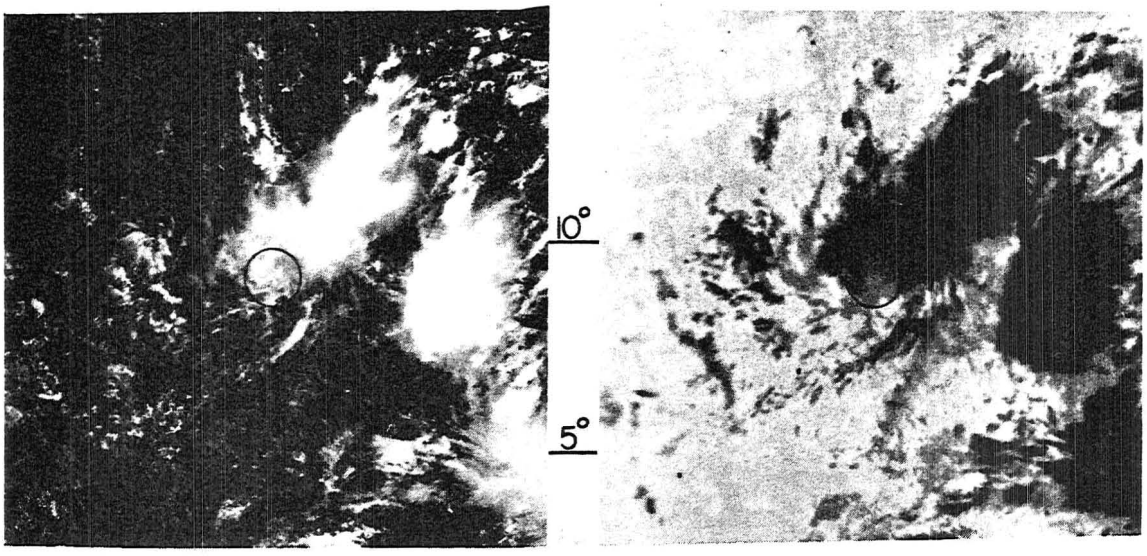

c c'

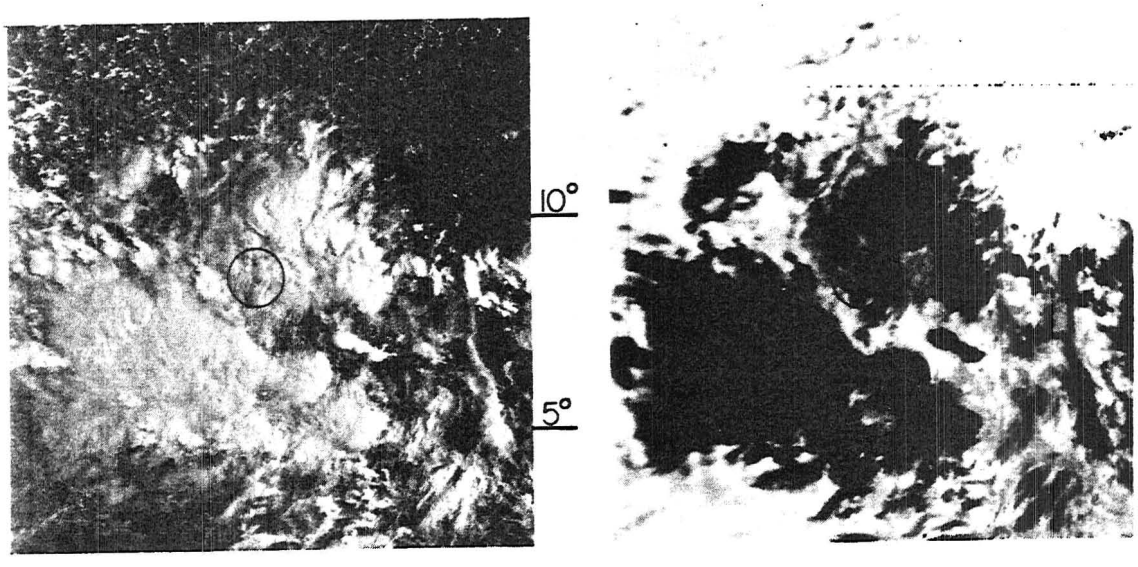

d d'

Fig. 38. Continued.

deep convection are properly orientated and maintained, an area of upper-level mass convergence appears to develop causing a concentrated area of subsidence warming and surface pressure falls adjacent to the deep convection. Lopez (1973) postulated that a forced subsidence warming mechanism might be a significant parameter in determining cyclone genesis. He stated:

> "There are reasons to believe that the broad-scale flow at the level of the disturbance's outflow (∿ 200 mb) might be the controlling factor. Thus, if the wind patterns at that level allows the outflow from the disturbance to be spread over a broad region, only gentle subsidence and warming will occur. However, if the upper-air wind pattern blocks somewhat the outflow; strong local subsidence and considerable warming might develop near the disturbance."

This mode of vortex initiation has also been recently discussed by Gray (1977).

7. SUMMARY

The most important findings as determined from a comparison of developing and non-developing disturbances are summarized:

1) Deep convection and disturbance vertical circulation is not well related to disturbance cyclone genesis potential.

2) Cirrus level outflow at 2-6° radius to the poleward side of the disturbance center was signficiantly greater with the developing disturbances. Unidirectional flow was present in the non-developing disturbances.

3) The day to day variability of deep convection was substantially larger than the mean cloudiness differences between systems.

4) Circulation centers of the pre-storm disturbances develop adjacent to or between areas of deep cumulus elements. A subsidence warming mechanism probably initiates this early stage warm core vortex.

5) Relative vorticity and vertical shear as determined by the rawinsonde composites demonstrated the most significant differences between disturbance classes. They are probably very significant parameters in cyclone genesis.

6) From the results of 1) and 5) it is concluded that tropical disturbance deep convection and vorticity are not well related.

ACKNOWLEDGEMENTS

The author would like to express his sincere gratitude to Professor William M. Gray for his guidance and support of this research project. The author is grateful to Major Charles Arnold who proposed the topic and for his assistance and encouragement throughout the study. I also thank Mr. Roger Whitcomb, Mr. Edwin Buzzell, and Mr. Charles Solomon for their assistance in computer programming and processing of the satellite and rawinsonde data. Many thanks are also due to Ms. Barbara Brumit and Ms. Dianne Schmitz for their untiring efforts in preparing the manuscript. The author would like to acknowledge the helpful discussions he has had on this subject with Dr. William M. Frank and Mr. John McBride.

This research has been sponsored by the United States Army Electronics, White Sands Missile Range, New Mexico, Grant Number DAEA 18-76-C-0050.

BIBLIOGRAPHY

Arnold, C. P., 1974: Tropical cyclone position and intensity analysis using satellite data. First Weather Wing Pamphlet, IWWP 105-10, Department of the Air Force, HQ 1st Weather Wing (MAC), 88 pp.

Arnold, C. P., 1977: Forthcoming CSU report on tropical cyclone convection using DMSP satellite data.

Colón, J. A. and W. R. Nightingale, 1963: Development of tropical cyclones in relation to circulation patterns at 200 mb level. Mon. Wea. Rev., 91, 329-336.

Computer Eye Handbook, 1974: First Edition, Spatial Data Systems, Inc., Goleta, CA, 42 pp.

Dickinson, L. G., S. E. Boselly and W. S. Burgmann, 1974: Defense Meteorological Satellite Program User's Guide. Air Weather Service Tech. Rept., 109 pp.

Dvorak, V. F., 1973: A technique for the analysis and forecasting of tropical cyclone intensities from satellite pictures. NOAA Technical Memorandum NESS 45 (Revision of NOAA TM NESS 36), U.S. Dept. of Commerce, Suitland, MD, 19 pp.

Dvorak, V. F., 1975: Tropical cyclone intensity analysis and forecasting from satellite imagery. Mon. Wea. Rev., 103, 420-430.

Fett, R. W., 1964: Aspects of hurricane structure: New model considerations suggested by TIROS and Project Mercury observations. Mon. Wea. Rev., 92, 43-60.

Fett, R. W., 1966: Upper-level structure of the formative tropical cyclone. Mon. Wea. Rev., 94, 9-18.

Fett, R. W. and S. Brand, 1975: Tropical cyclone movement forecasts based on observations from satellites. J. Appl. Meteor., 14, 452-465.

Fraedrich, K., E. Ruprecht and U. Trunte, 1976: Determination of the cirrus outflow divergence as seen by satellite. J. Appl. Meteor., 15, 1312-1316.

Frank, N. L. and H. M. Johnson, 1969: Vertical cloud systems over the tropical Atlantic during the 1967 hurricane season. Mon. Wea. Rev., 97, 124-129.

Frank, W. M., 1976: The structure and energetics of the tropical cyclone. Colo. State Univ., Atmos. Sci. Paper No. 258, Ft. Collins, CO, 3-12 pp.

Fritz, S., 1962: Satellite pictures and the origin of Hurricane Anna. Mon. Wea. Rev., 90, 507-513.

BIBLIOGRAPHY (cont'd)

Fritz, S., L. F. Hubert and A. Timchalk, 1966: Some inferences from satellite pictures of tropical disturbances. Mon. Wea. Rev., 94, 231-236.

GARP report on the first session of the study group on tropical disturbances (Madison, WI, 21 October - 8 November 1968), Joint GARP Organization Committee, WMO.

George, J. and W. M. Gray, 1976: Tropical cyclone motion and surrounding parameter relationships. J. Appl. Meteor., 15, 1252-1264.

Gray, W. M., 1968: Global view of the origin of tropical disturbances and storms. Mon. Wea. Rev., 96, 669-770.

Gray, W. M., 1975: Tropical cyclone genesis. Colo. State Univ., Atmos Sci. Paper No. 234, Ft. Collins, CO, 121 pp.

Gray, W. M., 1977: Tropical disturbance to cyclone transformation. (Submitted to J. Atmos. Sci.).

Hubert, L. F. and A. Timchalk, 1969: Estimating hurricane wind speeds from satellite pictures. Mon. Wea. Rev., 97, 382-383.

Jacobson, R. W., Jr. and W. M. Gray, 1976: Diurnal variation of oceanic deep cumulus convection, Paper I: Observational evidence, Paper II: Physical hypothesis. Colo. State Univ., Atmos. Sci. Paper No. 243, Ft. Collins, CO 106 pp.

Joint Typhoon Warning Center, 1972: Annual Typhoon Report, 1972. Fleet Weather Central, Guam, Mariana Islands, 134 pp.

Lopez, R. E., 1973: Cumulus convection and larger scale circulation. Part II: Cumulus and mesoscale interactions. Mon. Wea. Rev., 101, 856-870.

Malkus, J. A., C. Ronne and M. Chaffee, 1961: Cloud patterns in Hurricane Daisy. Tellus, 13, 8-30.

Martin, D. W. and V. E. Suomi, 1972: A satellite study of cloud clusters over the tropical North Atlantic ocean. Bull. Amer. Meteor. Soc., 53, 135-156.

Merritt, E. S., 1964: Easterly waves and perturbations, a reappraisal. J. Appl. Meteor., 3, 367-382.

Oliver, V. J. and R. K. Anderson, 1969: Circulation in the tropics as revealed by satellite data. Bull. Amer. Meteor. Soc., 50, 702-707.

BIBLIOGRAPHY (cont'd)

Riehl, H., 1954: Tropical Meteorology. McGraw-Hill, New York, 392 pp.

Riehl, H., 1975: Further studies on the origin of hurricanes. Colo. State Univ., Atmos. Sci. Paper No. 235, Ft. Collins, CO, 24 pp.

Ruprecht, E. and W. M. Gray, 1976: Analysis of satellite-observed tropical cloud clusters: Papers I and II. Tellus, 28, 391-425.

Sadler, J. C., 1964: Tropical cyclones of the eastern North Pacific as revealed by TIROS observations. J. Appl. Meteor., 3, 347-366.

Sadler, J. C., 1967: The tropical upper tropospheric trough as a secondary source of typhoons and a primary source of trade wind disturbances. Hawaii Institute of Geophysics, University of Hawaii, Final Report to Air Force Cambridge Research Laboratories, 44 pp.

Sadler, J. C., 1975: The monsoon circulation and cloudiness over the GATE area. Mon. Wea. Rev., 103, 369-387.

Sadler, J. C., 1976: A role of the tropical upper tropospheric trough in early season typhoon development. Mon. Wea. Rev., 104, 1266-1278.

Sikdar, D. N., V. E. Suomi and C. E. Anderson, 1970: Convective transport of mass and energy in severe storms over the United States - an estimate from geostationary altitude. Tellus, 22, 521-532.

Smith, C. L., E. J. Zipser, S. M. Daggupaty and L. Sapp, 1975: An experiment in tropical mesoscale analysis: Part 1 and 2. Mon. Wea. Rev., 103, 878-903.

Thompson, O. E. and J. Miller, 1976: Hurricane Carmen: August-September 1974 - development of a wave in the ITCZ. Mon. Wea. Rev., 104, 656-659.

Williams. K. T. and W. M. Gray, 1973: A statistical analysis of satellite-observed trade wind cloud clusters in the western North Pacific. Tellus, 25, 313-336.

Wright, S., 1976: The comparable development of Tropical Storm Hollie with a Gulf tropical disturbance. Mon. Wea. Rev., 104, 1451-1454.

Yanai, M., 1968: Evolution of a tropical disturbance in the Caribbean Sea region. J. Meteor. Soc. Japan, 46, 86-108.

Zehr, R., 1976: Tropical disturbance intensification. Colo. State Univ., Atmos. Sci. Paper No. 259, Ft. Collins, CO, 91 pp.

APPENDIX A

SATELLITE TRANSPARENCY GRIDDING

A unique feature of DMSP data is the ease with which it can be gridded. Figure A1 shows an example of an acetate grid used to position DMSP data. Note that the grid is longitudinally independent. All that is required to grid any satellite transparency is the longitude of nodal crossing and elapsed time since nodal crossing. Figure A1 gives an example of a gridded visual satellite transparency. Fiducial marks and time (seconds since nodal crossing) are displayed along the right hand side of the data. The longitude and time of nodal crossing is indicated in the legend (i.e., 163.43E and 2146 GMT). Gridding is accomplished by aligning the center of the fiducials along the solid line on the right-hand side of the grid. The 0000 time fiducial is centered on the dashed equator line. Solid lines indicate latitude and longitude, and satellite track is indicated by the dashed line directed north-northwest. Any visual feature should now be gridded with an accuracy of 1.5 n mi perpendicular to the satellite track and 3.0 n mi along the track at subpoint.

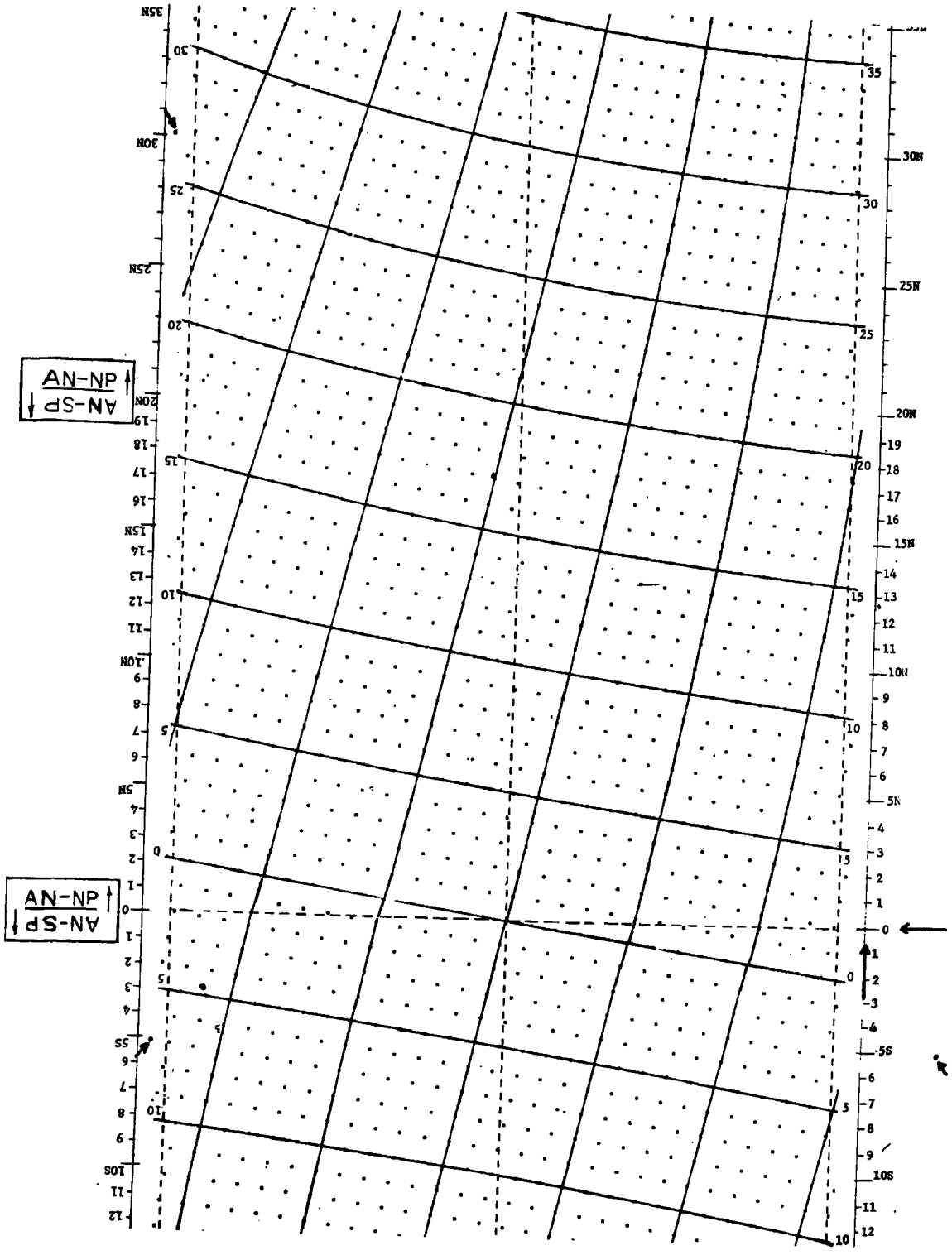

Fig. A1. Acetate grid used to position all visual and infrared DMSP film transparencies. Satellite subtrack is indicated by dashed vertical line.

APPENDIX B

OPTICAL DATA DIGITIZER DISPLAY SYSTEM (OD^3)

Area measurements of deep convection (digitized and traced) and cirrus were made utilizing the Colorado State University OD^3 system. This is more fully discussed in the Computer Eye Handbook. The system has the capability for digitizing transparencies. It consists of a scanner, video display, digitizer electronics, a computer controller, and a magnetic tape unit. The user has the option of either digitizing the data and storing it on magnetic tape to be processed later, or digitizing and processing the data directly by means of computer operation. The scanner consists of a black and white vidicon television camera which accurately senses the light emitted by the data sample being measured. The camera scans 480 lines (y-coordinate), each line containing 512 picture elements or pixels (x-coordinate). The video signal is digitized in 256 equal steps when the system is operated in linear mode. A digitized picture is thus an array (x,y) of numbers each representing the brightness relative to a specified density range. The percent areas covered by deep convection and cirrus, corresponding to a specified density range, are then determined within selected grid areas.

W. M. GRAY'S FEDERALLY SUPPORTED RESEARCH PROJECT REPORTS SINCE 1967

CSU Dept. of Atmos. Sci. Report No.	Report Title, Author, Date, Agency Support
104	The Mutual Variation of Wind, Shear, and Baroclinicity in the Cumulus Convective Atmosphere of the Hurricane (69pp). W. M. Gray. February 1967. NSF Support.
114	Global View of the Origin of Tropical Disturbances and Storms (105pp). W. M. Gray. October 1967. NSF Support.
116	A Statistical Study of the Frictional Wind Veering in the Planetary Boundary Layer (57pp). B. Mendenhall. December 1967. NSF and ESSA Support.
124	Investigation of the Importance of Cumulus Convection and Ventilation in Early Tropical Storm Development (88pp). R. Lopez. June 1968. ESSA Satellite Lab. Support.
Unnumbered	Role of Angular Momentum Transports in Tropical Storm Dissipation over Tropical Oceans (46pp). R. F. Wachtmann. December 1968. NSF and ESSA Support.
Unnumbered	Monthly Climatological Wind Fields Associated with Tropical Storm Genesis in the West Indies (34pp). J. W. Sartor. December 1968. NSF Support.
140	Characteristics of the Tornado Environment as Deduced from Proximity Soundings (55pp). T. G. Wills. June 1969. NOAA and NSF Support.
161	Statistical Analysis of Trade Wind Cloud Clusters of the Western North Pacific (80pp). K. Williams. June 1970. ESSA Satellite Lab. Support.
---	A Climatology of Tropical Cyclones and Disturbances of the Western Pacific with a Suggested Theory for Their Genesis/ Maintenance. W. M. Gray. NAVWEARSCHFAC Technical Paper No. 19-70 (225pp). November 1970. (Available from U.S. Navy, Monterey, CA). U.S. Navy Support.
179	A Diagnostic Study of the Planetary Boundary Layer over the Oceans (95pp). W. M. Gray. February 1972. Navy and NSF Support.
182	The Structure and Dynamics of the Hurricane's Inner Core Area (105pp). D. J. Shea. April 1972. NOAA and NSF Support.
188	Cumulus Convection and Larger-Scale Circulation, Part I: A Parametric Model of Cumulus Convection (100pp). R. E. Lopez. June 1972. NSF Support.

CSU Dept. of Atmos. Sci. Report No.	Report Title, Author, Date, Agency Support
189	Cumulus Convection and Larger-Scale Circulations, Part II: Cumulus and Meso-Scale Interactions (63pp). R. E. Lopez. June 1972. NSF Support.
190	Cumulus Convection and Larger-Scale Circulations, Part III: Broadscale and Meso-Scale Considerations (80pp). W. M. Gray. July 1972. NOAA-NESS.
195	Characteristics of Carbon Black Dust as a Tropospheric Heat Source for Weather Modification (55pp). W. M. Frank. January 1973. NSF Support.
196	Feasibility of Beneficial Hurricane Modification by Carbon Black Seeding (130pp). W. M. Gray. April 1973. NOAA Support.
199	Variability of Planetary Boundary Layer Winds (157pp). L. R. Hoxit. May 1973. NSF Support.
200	Hurricane Spawned Tornadoes (57pp). D. J. Novlan. May 1973. NOAA and NSF Support.
212	A Study of Tornado Proximity Data and an Observationally Derived Model of Tornado Genesis (101pp). R. Maddox. November 1973. NOAA Support.
219	Analysis of Satellite Observed Tropical Cloud Clusters (91 pp). E. Ruprecht and W. M. Gray. May 1974. NOAA-NESS Support.
224	Precipitation Characteristics in the Northeast Brazil Dry Region (56pp). R. P. L. Ramos. May 1974. NSF Support.
225	Weather Modification through Carbon Dust Absorption of Solar Energy (190pp). W. M. Gray, W. M. Frank, M. L. Corrin, and C. A. Stokes. July 1974.
234	Tropical Cyclone Genesis (121pp). W. M. Gray. March 1975. NSF Support.
---	Tropical Cyclone Genesis in the Western North Pacific (66pp). W. M. Gray. March 1975. U.S. Navy Environmental Prediction Research Facility Report. Technical Paper No. 16-75. (Available from the U.S. Navy, Monterey, CA). Navy Support.
241	Tropical cyclone Motion and Surrounding Parameter Relationships (105pp). J. E. George. December 1975. NOAA Support.

CSU Dept. of Atmos. Sci. Report No.	Report Title, Author, Date, Agency Support
243	Diurnal Variation of Oceanic Deep Cumulus Convection. Paper I: Observational Evidence, Paper II: Physical Hypothesis (106pp). R. W. Jacobson, Jr. and W. M. Gray. February, 1976. NOAA NESS Support.
257	Data Summary of NOAA's Hurricane Inner-Core Radial Leg Flight Penetrations 1957-1967, and 1969 (245pp). W. M. Gray and D. J. Shea. October, 1976. NSF and NOAA Support.
258	The Structure and Energetics of the Tropical Cyclone (180 pp). W. M. Frank. October, 1976. NOAA (NHEML), NOAA (NESS) and NSF Support.
259	Typhoon Genesis and Pre-typhoon Cloud Clusters (79pp). R. M. Zehr. November, 1976.
Unnumbered	Severe Thunderstorm Wind Gusts (81pp). G. W. Walters. December, 1976. NSF Support.
262	Diurnal Variation of the Tropospheric Energy Budget (141 pp). G. S. Foltz. November, 1976. NSF Support.

BIBLIOGRAPHIC DATA SHEET	1. Report No. CSU-ATSP-274	2.	3. Recipient's Accession No.
4. Title and Subtitle	COMPARISON OF DEVELOPING VS. NON-DEVELOPING TROPICAL DISTURBANCES		5. Report Date July, 1977 6.
7. Author(s)	Steven L. Erickson P.I. (William M. Gray)		8. Performing Organization Rept. No. 274
9. Performing Organization Name and Address Atmospheric Science Department Colorado State University Fort Collins, Colorado 80523			10. Project/Task/Work Unit No. 11. Contract/Grant No. DAEA 18-76-C-0050
12. Sponsoring Organization Name and Address United States Army Electronics White Sands Missile Range New Mexico			13. Type of Report & Period Covered Project Report 14.

15. Supplementary Notes

16. Abstracts Developing and non-developing weatern North Pacific tropical disturbances are investigated and compared utilizing Defense Meteorological Satellite Program (DMSP) and rawinsonde data. Quantitative measurements of deep convection and cirrus amounts from the satellite visual and infrared data indicates that no large deep-convective difference exists between these two classes of disturbances. In addition, the daily variability of deep convection was determined to be large in both the developing and non-developing disturbances. Implications are that the amount and intensity of deep convection is not well related to disturbance tropical storm genesis potential. Genesis appears to be related to the special positioning of the deep convection and surrounding wind fields. When genesis occurs, the deep convection appears to act indirectly to warm the tropical disturbance by means of dynamically forced subsidence. Documentation is provided to support this hypothesis.

17. Key Words and Document Analysis. 17a. Descriptors

Tropical Disturbances
Tropical Cyclones

17b. Identifiers/Open-Ended Terms

17c. COSATI Field/Group

18. Availability Statement	19. Security Class (This Report) UNCLASSIFIED	21. No. of Pages 81
	20. Security Class (This Page) UNCLASSIFIED	22. Price

FORM NTIS-35 (Rev. 3-72)